

## Chapter 2

# Fifth order solution of halo orbits in CRTBP for Sun-Earth and Earth -Moon systems

### 2.1 Introduction

The existence of equilibrium points of CRTBP was established by Euler and Lagrange in the 18<sup>th</sup> century but its first application was suggested in 1950 by Arthur C. Clarke. He proposed that for relaying radio and TV broadcasts from the Earth to colonists on the far side of the Moon, the Earth-Moon  $L_2$  point would be an ideal place. In 1966, Robert Farquhar identified trajectories around Earth-Moon  $L_2$  in which a communication satellite could be positioned to maintain a constant connection between the Earth and the far side of the Moon (Farquhar (1966)). He called these orbits as halo orbits because from the Earth, these orbits appeared to be a halo around the Moon.

Halo family is a family of three dimensional periodic orbits around collinear Lagrangian points which arise as a bifurcation from the planar Lyapunov orbits. A satellite placed in a halo orbit can serve many scientific purposes. In any Sun-Planet system, the Lagrangian point  $L_1$  lies between the Sun and the planet. A satellite placed in a halo orbit around  $L_1$  remains in direct contact with the Sun without any occultation or eclipse. The space weather is constantly influenced by the radiation, solar wind and magnetic fields of the Sun. The solar wind along with other explosive events like Coronal Mass Ejection (CME) affects the space weather and the nature of magnetic field and it also changes charge particle environment near the planet. Since the atmosphere and magnetic field of a planet like Earth acts as a protective shield, many particles and fields do not reach the surface of the planet. So, the study of such particles, magnetic field and space weather near a planet can be done from the space. For accomplishing such scientific goals, halo orbits are very useful. International Sun-Earth Explorer-3

(ISEE-3) was the first halo orbit mission. It was placed in a halo orbit around the Sun-Earth  $L_1$  for collecting data on solar wind conditions upstream from Earth. Solar and Heliospheric Observatory (SOHO) is another famous halo orbit mission around the Sun-Earth  $L_1$ . The aim of this mission was to study the internal structure, outer atmosphere as well as the solar wind blown by the Sun.

Indian Space Research Organisation (ISRO) has planned Aditya  $L_1$  mission to study the Sun. It is the first space based observatory class Indian solar mission to study the Sun. It will be placed in a halo orbit around the Sun-Earth  $L_1$ . The major objectives of this mission are ([https://www.isro.gov.in/Aditya\\_L1.html](https://www.isro.gov.in/Aditya_L1.html)):

- To understand the coronal heating and solar wind acceleration.
- To understand initiation of Coronal Mass Ejection (CME), flares and near Earth space weather.
- To understand the coupling and dynamics of the solar atmosphere.
- To understand the solar wind distribution and temperature anisotropy.

Aditya  $L_1$  mission carries seven scientific payloads which are all indigenous.

A satellite placed in a halo orbit around Sun-Earth  $L_2$  can be used for space based observations. James Webb Space Telescope (JWST) is the most recent Sun-Earth  $L_2$  halo orbit mission ([https://www.esa.int/ESA\\_Multimedia/Images/2022/03/The\\_orbits\\_of\\_Gaia\\_and\\_Webb](https://www.esa.int/ESA_Multimedia/Images/2022/03/The_orbits_of_Gaia_and_Webb)). The major objectives of this mission are (<https://nssdc.gsfc.nasa.gov/nmc/spacecraft/display.action?id=2021-130A>):

- To study the earliest phases of the universe.
- To study how galaxies were formed.
- To study how stars and protoplanetary systems develop.
- To observe planets in our own as well as other solar systems.

JWST was launched on December 25, 2021 and it is planned to operate for 10 years. It carries four science instruments: a Near-IR Camera (NIRCam), a Near-IR Spectrograph (NIRSpec), a Near-IR Tunable Filter Imager (TFI) and a Mid-IR Instrument (MIRI). The near IR instruments operate in the wavelength from 0.6 to 5.0 microns and the mid-IR instruments operate in the wavelength from 5.0 to 29.0 microns.

As indicated by Farquhar, the Earth-Moon  $L_2$  halo orbit can be used for placing a communication satellite for establishing connection with the far side of the Moon.

In 2018, China National Space Administration (CNSA) launched Queqiao, a communication relay satellite for its Chang's-4 lunar far side mission. Queqiao entered in a halo orbit around the Earth-Moon  $L_2$  on June 14, 2018 and established communications between Chang'e-4 lander on the far side of the Moon and the Earth (<https://nssdc.gsfc.nasa.gov/nmc/spacecraft/display.action?id=QUEQIAO>).

In 1980, Richardson (1980) gave an approximate third order analytical solution using Lindstedt-Poincaré method for finding halo orbits in the classical CRTBP. Recently, Tiwary and Kushvah (2015) derived an analytical guess for halo orbits around  $L_1$  and  $L_2$  in the photogravitational Sun-Earth system with oblateness by considering the fourth order approximate solution using Lindstedt-Poincaré technique. In this chapter, fifth order approximation using Lindstedt-Poincaré method is computed and it is used for obtaining a first guess for halo orbits around  $L_1$ ,  $L_2$  and  $L_3$  by considering both the primaries as source of radiation as well as oblate spheroids. This analytical solution is revised using the numerical method of differential correction for getting more precise initial state vector for halo orbits. Also, the effects of perturbations due to radiation pressure and oblateness of the primaries on parameters of halo orbits are studied.

## 2.2 Computation of halo orbits

For finding halo orbits, the origin of the coordinate system is shifted to the corresponding Lagrangian point from the barycentre of the primaries and the equations of motion in the vicinity of the Lagrangian point are obtained. Also, in the translated system, new coordinates are normalized by dividing them with the quantity  $\gamma$ , the distance between  $L_i$  ( $i = 1, 2, 3$ ) and the nearest primary. For  $L_1$  and  $L_2$ ,  $\gamma$  is the distance between  $L_i$  ( $i = 1, 2$ ) and  $P_2$  and for  $L_3$ ,  $\gamma$  is the distance between  $L_3$  and  $P_1$ . Then the new coordinates  $(\tilde{x}, \tilde{y}, \tilde{z})$  are (Koon et al. (2011))

$$\begin{aligned} \tilde{x} &= \begin{cases} \frac{1}{\gamma}(x + \mu - 1 \pm \gamma), & \text{for } L_1 \text{ and } L_2 \\ \frac{1}{\gamma}(x + \mu + \gamma), & \text{for } L_3 \end{cases} \\ \tilde{y} &= \frac{1}{\gamma}y, \\ \tilde{z} &= \frac{1}{\gamma}z. \end{aligned} \tag{2.1}$$

In the first equation, the upper sign corresponds to  $L_1$  and the lower sign corresponds to  $L_2$ . Since the variables are normalized in the new coordinate system, the distance

between the Lagrangian point and the nearest primary is unity.

Using transformation (2.1) into system (1.6), the equations of motion get transformed to

$$\begin{aligned}\ddot{\tilde{x}} - 2n\dot{\tilde{y}} &= \frac{1}{\gamma^2}\Omega_{\tilde{x}}, \\ \ddot{\tilde{y}} + 2n\dot{\tilde{x}} &= \frac{1}{\gamma^2}\Omega_{\tilde{y}}, \\ \ddot{\tilde{z}} &= \frac{1}{\gamma^2}\Omega_{\tilde{z}},\end{aligned}\tag{2.2}$$

where

$$\Omega = \frac{n^2}{2} \left[ (\gamma\tilde{x} + 1 - \mu \mp \gamma)^2 + (\gamma\tilde{y})^2 \right] + \frac{(1-\mu)q_1}{R_1} + \frac{(1-\mu)q_1A_1}{2R_1^3} + \frac{\mu q_2}{R_2} + \frac{\mu q_2A_2}{2R_2^3}\tag{2.3}$$

and

$$R_1 = \sqrt{(\gamma\tilde{x} + 1 \mp \gamma)^2 + (\gamma\tilde{y})^2 + (\gamma\tilde{z})^2},\tag{2.4}$$

$$R_2 = \sqrt{(\gamma\tilde{x} \mp \gamma)^2 + (\gamma\tilde{y})^2 + (\gamma\tilde{z})^2},\tag{2.5}$$

for  $L_1$  and  $L_2$ . For  $L_3$ ,

$$\Omega = \frac{n^2}{2} \left[ (\gamma\tilde{x} - \mu - \gamma)^2 + (\gamma\tilde{y})^2 \right] + \frac{(1-\mu)q_1}{R_1} + \frac{(1-\mu)q_1A_1}{2R_1^3} + \frac{\mu q_2}{R_2} + \frac{\mu q_2A_2}{2R_2^3},\tag{2.6}$$

$$R_1 = \sqrt{(\gamma\tilde{x} - \gamma)^2 + (\gamma\tilde{y})^2 + (\gamma\tilde{z})^2},\tag{2.7}$$

$$R_2 = \sqrt{(\gamma\tilde{x} - \gamma - 1)^2 + (\gamma\tilde{y})^2 + (\gamma\tilde{z})^2}.\tag{2.8}$$

Suppose  $d$  denotes the distance between the two points  $(\tilde{x}, \tilde{y}, \tilde{z})$  and  $(A, B, C)$  in Euclidean space. Then

$$d = \sqrt{(\tilde{x} - A)^2 + (\tilde{y} - B)^2 + (\tilde{z} - C)^2}\tag{2.9}$$

which gives

$$\begin{aligned}\frac{1}{d} &= \frac{1}{\sqrt{(\tilde{x} - A)^2 + (\tilde{y} - B)^2 + (\tilde{z} - C)^2}}, \\ &= \frac{1}{\sqrt{(A^2 + B^2 + C^2) + (\tilde{x}^2 + \tilde{y}^2 + \tilde{z}^2) - 2(A\tilde{x} + B\tilde{y} + C\tilde{z})}}, \\ &= \frac{1}{\sqrt{A^2 + B^2 + C^2} \sqrt{1 - 2\left(\frac{A\tilde{x} + B\tilde{y} + C\tilde{z}}{A^2 + B^2 + C^2}\right) + \left(\frac{\tilde{x}^2 + \tilde{y}^2 + \tilde{z}^2}{A^2 + B^2 + C^2}\right)}}.\end{aligned}\tag{2.10}$$

The generating function for the classical Legendre polynomials is (Rainville (1961, p.130)):

$$(1 - 2xt + t^2)^{-1/2} = \sum_{m=0}^{\infty} P_m(x)t^m, \quad (2.11)$$

where  $|t| < 1$  and  $x \in \mathbb{R}$ .

The multiple of  $(A^2 + B^2 + C^2)^{-1/2}$  in (2.10) may be compared with  $(1 - 2xt + t^2)^{-1/2}$ , where

$$x = \frac{A\tilde{x} + B\tilde{y} + C\tilde{z}}{\sqrt{\tilde{x}^2 + \tilde{y}^2 + \tilde{z}^2}\sqrt{A^2 + B^2 + C^2}}, \quad t = \sqrt{\frac{\tilde{x}^2 + \tilde{y}^2 + \tilde{z}^2}{A^2 + B^2 + C^2}}.$$

With these choices, it turns out to be the generating function of the Legendre polynomials  $P_m(x)$ . Thus,

$$\frac{1}{d} = \frac{1}{\sqrt{A^2 + B^2 + C^2}} \sum_{m=0}^{\infty} P_m\left(\frac{A\tilde{x} + B\tilde{y} + C\tilde{z}}{\sqrt{\tilde{x}^2 + \tilde{y}^2 + \tilde{z}^2}\sqrt{A^2 + B^2 + C^2}}\right) \left(\frac{\tilde{x}^2 + \tilde{y}^2 + \tilde{z}^2}{A^2 + B^2 + C^2}\right)^{m/2}.$$

Using the notations  $\rho^2 = \tilde{x}^2 + \tilde{y}^2 + \tilde{z}^2$  and  $D^2 = A^2 + B^2 + C^2$ , above expression takes the elegant form (Koon et al. (2011, p.146)):

$$\frac{1}{d} = \frac{1}{D} \sum_{m=0}^{\infty} \left(\frac{\rho}{D}\right)^m P_m\left(\frac{A\tilde{x} + B\tilde{y} + C\tilde{z}}{\rho D}\right). \quad (2.12)$$

The terms  $1/R_1, 1/R_2, 1/R_1^3$  and  $1/R_2^3$  in (2.3) and (2.6) are expanded using Legendre polynomials. For series expansion of  $1/R_1^3$  and  $1/R_2^3$ , the Cauchy product of series is used and in each expansion, the terms containing the product of Legendre polynomials are neglected. For  $R_1$  in (2.4), a comparison between (2.4) and (2.9) gives

$$A = -\frac{1}{\gamma} \pm 1, \quad B = 0, \quad C = 0, \quad \text{hence } D = \frac{1}{\gamma} \mp 1. \quad \text{From (2.12),}$$

$$\begin{aligned} \frac{1}{R_1} &= \frac{1}{\gamma \left(\frac{1}{\gamma} \mp 1\right)} \sum_{m=0}^{\infty} \left(\frac{\rho}{\left(\frac{1}{\gamma} \mp 1\right)}\right)^m P_m\left(\frac{\left(-\frac{1}{\gamma} \pm 1\right) \tilde{x}}{\rho \left(\frac{1}{\gamma} \mp 1\right)}\right) \\ &= \frac{1}{\gamma} \sum_{m=0}^{\infty} \left(\frac{\gamma}{1 \mp \gamma}\right)^{m+1} (-1)^m P_m\left(\frac{\tilde{x}}{\rho}\right) \rho^m. \end{aligned}$$

It can be observed that  $\rho/D < 1$  as  $\gamma < 1/2$  implying  $\left(\frac{1}{\gamma} \mp 1\right)^{-1} > 1$  which justifies  $|t| < 1$ . In a similar manner,

$$\begin{aligned}\frac{1}{R_2} &= \frac{1}{\gamma} \sum_{m=0}^{\infty} (\pm 1)^m P_m\left(\frac{\tilde{x}}{\rho}\right) \rho^m, \\ \frac{1}{R_1^3} &= \frac{1}{(1 \mp \gamma)^3} + \frac{1}{\gamma^3} \sum_{m=1}^{\infty} 3 \left(\frac{\gamma}{1 \mp \gamma}\right)^{m+3} (-1)^m P_m\left(\frac{\tilde{x}}{\rho}\right) \rho^m, \\ \frac{1}{R_2^3} &= \frac{1}{\gamma^3} + \sum_{m=1}^{\infty} \frac{3(\pm 1)^m}{\gamma^3} P_m\left(\frac{\tilde{x}}{\rho}\right) \rho^m,\end{aligned}$$

for  $L_1$  and  $L_2$ . For  $L_3$ ,

$$\begin{aligned}\frac{1}{R_1} &= \frac{1}{\gamma} \sum_{m=0}^{\infty} P_m\left(\frac{\tilde{x}}{\rho}\right) \rho^m, \\ \frac{1}{R_2} &= \sum_{m=0}^{\infty} \frac{\gamma^m}{(1 + \gamma)^{m+1}} P_m\left(\frac{\tilde{x}}{\rho}\right) \rho^m, \\ \frac{1}{R_1^3} &= \frac{1}{\gamma} \left[ 1 + 3 \sum_{m=1}^{\infty} P_m\left(\frac{\tilde{x}}{\rho}\right) \rho^m \right], \\ \frac{1}{R_2^3} &= \frac{1}{(1 + \gamma)^3} + 3 \sum_{m=1}^{\infty} \frac{\gamma^m}{(1 + \gamma)^{m+3}} P_m\left(\frac{\tilde{x}}{\rho}\right) \rho^m.\end{aligned}$$

Substituting the expansions for  $1/R_i$  and  $1/R_i^3$ ,  $i = 1, 2$ , in equations of motion and collecting all linear terms on left and non-linear terms on right, we get,

$$\begin{aligned}\ddot{\tilde{x}} - 2n\dot{\tilde{y}} - (n^2 + 2C_2)\tilde{x} &= \frac{\partial}{\partial \tilde{x}} \sum_{m \geq 3} C_m \rho^m P_m\left(\frac{\tilde{x}}{\rho}\right), \\ \ddot{\tilde{y}} + 2n\dot{\tilde{x}} + (C_2 - n^2)\tilde{y} &= \frac{\partial}{\partial \tilde{y}} \sum_{m \geq 3} C_m \rho^m P_m\left(\frac{\tilde{x}}{\rho}\right), \\ \ddot{\tilde{z}} + C_2\tilde{z} &= \frac{\partial}{\partial \tilde{z}} \sum_{m \geq 3} C_m \rho^m P_m\left(\frac{\tilde{x}}{\rho}\right),\end{aligned} \tag{2.13}$$

where

$$C_m = \frac{1}{\gamma^3} \left[ (-1)^m q_1 (1 - \mu) \left( \frac{\gamma}{1 \mp \gamma} \right)^{m+1} \left( 1 + \frac{3A_1}{2(1 \mp \gamma)^2} \right) + (\pm 1)^m \mu q_2 \left( 1 + \frac{3A_2}{2\gamma^2} \right) \right], \quad (2.14)$$

with  $m \geq 1$ , for  $L_1$  and  $L_2$ . For  $L_3$ ,

$$C_m = \frac{1}{\gamma^3} \left[ (1 - \mu) q_1 \left( 1 + \frac{3A_1}{2\gamma^2} \right) + \frac{\mu q_2 \gamma^{m+1}}{(1 + \gamma)^{m+1}} \left( 1 + \frac{3A_2}{2(1 + \gamma)^2} \right) \right], \quad m \geq 1. \quad (2.15)$$

The solution of the linearized system corresponding to system (2.13), obtained by neglecting all non-linear terms appearing on the right side of the system (2.13), is (Koon et al. (2011) and Tiwary and Kushvah (2015))

$$\begin{aligned} \tilde{x}(t) &= a_1 e^{\alpha t} + a_2 e^{-\alpha t} + a_3 \cos \lambda t + a_4 \sin \lambda t, \\ \tilde{y}(t) &= -k_1 a_1 e^{\alpha t} + k_1 a_2 e^{-\alpha t} - k_2 a_3 \sin \lambda t + k_2 a_4 \cos \lambda t, \\ \tilde{z}(t) &= a_5 \cos \sqrt{C_2} t + a_6 \sin \sqrt{C_2} t, \end{aligned}$$

where  $a_i, i = 1$  to  $6$ , are arbitrary constants and the parameters  $\alpha, \lambda, k_1$  and  $k_2$  are given by

$$\begin{aligned} \alpha &= \sqrt{\frac{-(2n^2 - C_2) + \sqrt{9C_2^2 - 8n^2C_2}}{2}}, \\ \lambda &= \sqrt{\frac{2n^2 - C_2 + \sqrt{9C_2^2 - 8n^2C_2}}{2}}, \\ \kappa_1 &= \frac{(2C_2 + n^2) - \alpha^2}{2n\alpha}, \\ \kappa_2 &= \frac{(2C_2 + n^2) + \lambda^2}{2n\lambda}. \end{aligned}$$

The solution of the linearized system is unbounded because the solution of characteristic equation has two real roots which are equal in magnitude and opposite in sign. By taking  $a_1 = a_2 = 0, a_3 = -A_{\tilde{x}} \cos \phi, a_4 = A_{\tilde{x}} \sin \phi, a_5 = A_{\tilde{z}} \sin \psi, a_6 = A_{\tilde{z}} \cos \psi$  as an initial condition, a bounded solution can be obtained in the form (Koon et al. (2011) and Tiwary and Kushvah (2015)):

$$\begin{aligned} \tilde{x}(t) &= -A_{\tilde{x}} \cos(\lambda t + \phi), \\ \tilde{y}(t) &= \kappa A_{\tilde{x}} \sin(\lambda t + \phi), \\ \tilde{z}(t) &= A_{\tilde{z}} \sin(\sqrt{C_2} t + \psi), \end{aligned}$$

where  $A_{\tilde{x}}$  and  $A_{\tilde{z}}$  are amplitudes;  $\lambda$  and  $\sqrt{C_2}$  are the frequencies;  $\phi$  and  $\psi$  are phases of the in-plane and out-of-plane motions, respectively, and  $\kappa_2$  is replaced by  $\kappa$ . The in-plane and out-of-plane frequencies of linearized motion are different. If the ratio of these frequencies is irrational, then quasi-periodic orbits are obtained. For computing periodic orbits, the last equation of (2.13) is expressed as

$$\ddot{\tilde{z}} + \lambda^2 \tilde{z} = \frac{\partial}{\partial \tilde{z}} \sum_{m \geq 3} C_m \rho^m P_m \left( \frac{\tilde{x}}{\rho} \right) + \Delta \tilde{z}, \quad (2.16)$$

where  $\Delta = \lambda^2 - C_2$  is called frequency correction term and  $\Delta = \mathcal{O}(\epsilon^2)$ . Expanding the series on the right hand side of the system (2.13) and equation (2.16) upto  $m = 6$  for acquiring the fifth order approximate solution, we get

$$\begin{aligned} \ddot{\tilde{x}} - 2n\dot{\tilde{y}} - (n^2 + 2C_2)\tilde{x} &= \frac{3}{2}C_3(2\tilde{x}^2 - \tilde{y}^2 - \tilde{z}^2) + 2C_4\tilde{x}(2\tilde{x}^2 - 3\tilde{y}^2 - 3\tilde{z}^2) \\ &+ \frac{5}{8}C_5[8\tilde{x}^2\{\tilde{x}^2 - 3(\tilde{y}^2 + \tilde{z}^2)\} + 3(\tilde{y}^2 + \tilde{z}^2)^2] \\ &+ 3C_6 \left[ 2\tilde{x}^3\{\tilde{x}^2 - 5(\tilde{y}^2 + \tilde{z}^2)\} + \frac{15}{4}\tilde{x}(\tilde{y}^2 + \tilde{z}^2)^2 \right], \\ \ddot{\tilde{y}} + 2n\dot{\tilde{x}} + (C_2 - n^2)\tilde{y} &= -3C_3\tilde{x}\tilde{y} - \frac{3}{2}C_4\tilde{y}(4\tilde{x}^2 - \tilde{y}^2 - \tilde{z}^2) \\ &- \frac{5}{2}C_5\tilde{x}\tilde{y}(4\tilde{x}^2 - 3\tilde{y}^2 - 3\tilde{z}^2) \\ &+ \frac{15}{2}C_6 \left[ \tilde{x}^2\tilde{y}\{-2\tilde{x}^2 + 3(\tilde{y}^2 + \tilde{z}^2)\} - \frac{1}{4}\tilde{y}(\tilde{y}^2 + \tilde{z}^2)^2 \right], \\ \ddot{\tilde{z}} + \lambda^2 \tilde{z} &= \Delta \tilde{z} - 3C_3\tilde{x}\tilde{z} - \frac{3}{2}C_4\tilde{z}(4\tilde{x}^2 - \tilde{y}^2 - \tilde{z}^2) \\ &- \frac{5}{2}C_5\tilde{x}\tilde{z}(4\tilde{x}^2 - 3\tilde{y}^2 - 3\tilde{z}^2) \\ &+ \frac{15}{2}C_6 \left[ \tilde{x}^2\tilde{z}\{-2\tilde{x}^2 + 3(\tilde{y}^2 + \tilde{z}^2)\} - \frac{1}{4}\tilde{z}(\tilde{y}^2 + \tilde{z}^2)^2 \right] \end{aligned} \quad (2.17)$$

Lindstedt-Poincaré method is applied to system (2.17) for getting analytic solution.

### 2.2.1 Analytic solutions of halo orbits around $L_1$ , $L_2$ and $L_3$

In successive approximations, the non-linear factors in system (2.17) generate secular terms. To alter the frequency of the solution of the non-linear system, a new independent variable  $\tau = \omega t$  is introduced. Then

$$\frac{d(\cdot)}{dt} = \omega \frac{d(\cdot)}{d\tau}, \quad \frac{d^2(\cdot)}{dt^2} = \omega^2 \frac{d^2(\cdot)}{d\tau^2}.$$

Expressing system (2.17) in terms of new variable  $\tau$ ,

$$\begin{aligned}
 \omega^2 \tilde{x}'' - 2n\omega \tilde{y}' - (n^2 + 2C_2)\tilde{x} &= \frac{3}{2}C_3(2\tilde{x}^2 - \tilde{y}^2 - \tilde{z}^2) \\
 &+ 2C_4\tilde{x}(2\tilde{x}^2 - 3\tilde{y}^2 - 3\tilde{z}^2) \\
 &+ \frac{5}{8}C_5[8\tilde{x}^2\{\tilde{x}^2 - 3(\tilde{y}^2 + \tilde{z}^2)\} + 3(\tilde{y}^2 + \tilde{z}^2)^2] \\
 &+ 3C_6\left[2\tilde{x}^3\{\tilde{x}^2 - 5(\tilde{y}^2 + \tilde{z}^2)\}\right. \\
 &\left.+ \frac{15}{4}\tilde{x}(\tilde{y}^2 + \tilde{z}^2)^2\right], \\
 \omega^2 \tilde{y}'' + 2n\omega \tilde{x}' + (C_2 - n^2)\tilde{y} &= -3C_3\tilde{x}\tilde{y} - \frac{3}{2}C_4\tilde{y}(4\tilde{x}^2 - \tilde{y}^2 - \tilde{z}^2) \\
 &- \frac{5}{2}C_5\tilde{x}\tilde{y}(4\tilde{x}^2 - 3\tilde{y}^2 - 3\tilde{z}^2) \\
 &+ \frac{15}{2}C_6\left[\tilde{x}^2\tilde{y}\{-2\tilde{x}^2 + 3(\tilde{y}^2 + \tilde{z}^2)\}\right. \\
 &\left.- \frac{1}{4}\tilde{y}(\tilde{y}^2 + \tilde{z}^2)^2\right], \\
 \omega^2 \tilde{z}'' + \lambda^2 \tilde{z} &= -3C_3\tilde{x}\tilde{z} - \frac{3}{2}C_4\tilde{z}(4\tilde{x}^2 - \tilde{y}^2 - \tilde{z}^2) \\
 &- \frac{5}{2}C_5\tilde{x}\tilde{z}(4\tilde{x}^2 - 3\tilde{y}^2 - 3\tilde{z}^2) \\
 &+ \frac{15}{2}C_6\left[\tilde{x}^2\tilde{z}\{-2\tilde{x}^2 + 3(\tilde{y}^2 + \tilde{z}^2)\}\right. \\
 &\left.- \frac{1}{4}\tilde{z}(\tilde{y}^2 + \tilde{z}^2)^2\right] + \Delta\tilde{z},
 \end{aligned} \tag{2.18}$$

where ' denotes derivative with respect to  $\tau$ . Considering the solution of the system (2.18) in the perturbation form as given in equations (1.41)-(1.44) and truncating series in these expressions after first five terms for fifth order solution, the final solution will be of the form:

$$\begin{aligned}
 \tilde{x}(\tau) &= \epsilon\tilde{x}_1(\tau) + \epsilon^2\tilde{x}_2(\tau) + \epsilon^3\tilde{x}_3(\tau) + \epsilon^4\tilde{x}_4(\tau) + \epsilon^5\tilde{x}_5(\tau), \\
 \tilde{y}(\tau) &= \epsilon\tilde{y}_1(\tau) + \epsilon^2\tilde{y}_2(\tau) + \epsilon^3\tilde{y}_3(\tau) + \epsilon^4\tilde{y}_4(\tau) + \epsilon^5\tilde{y}_5(\tau), \\
 \tilde{z}(\tau) &= \epsilon\tilde{z}_1(\tau) + \epsilon^2\tilde{z}_2(\tau) + \epsilon^3\tilde{z}_3(\tau) + \epsilon^4\tilde{z}_4(\tau) + \epsilon^5\tilde{z}_5(\tau),
 \end{aligned} \tag{2.19}$$

with

$$\omega = 1 + \epsilon\omega_1 + \epsilon^2\omega_2 + \epsilon^3\omega_3 + \epsilon^4\omega_4. \tag{2.20}$$

Substituting the expressions (2.19) with (2.20) into system (2.18) and equating coefficients of  $\epsilon^5$  by incorporating all the solutions and constraints used upto the fourth

order solution, the fifth order equations are obtained as:

$$\begin{aligned}\tilde{x}_5'' - 2n\tilde{y}_5' - (n^2 + 2C_2)\tilde{x}_5 &= \gamma_{51}, \\ \tilde{y}_5'' + 2n\tilde{x}_5' + (C_2 - n^2)\tilde{y}_5 &= \gamma_{52}, \\ \tilde{z}_5'' + \lambda^2\tilde{z}_5 &= f_3, \quad p = 1, 3,\end{aligned}\tag{2.21}$$

where

$$\begin{aligned}\gamma_{51} &= [v_4 + 2\lambda A_{\tilde{x}}\omega_4(nk - \lambda)] \cos \tau_1 + \gamma_8 \cos 3\tau_1 + \gamma_9 \cos 5\tau_1, \\ \gamma_{52} &= [v_5 + 2\lambda A_{\tilde{x}}\omega_4(\lambda k - n)] \sin \tau_1 + \beta_9 \sin 3\tau_1 + \beta_{10} \sin 5\tau_1, \\ f_3 &= [v_6 \pm 2\omega_4\lambda^2 A_{\tilde{z}}] \cos \tau_1 + \delta_8 \cos 3\tau_1 + \delta_9 \cos 5\tau_1\end{aligned}$$

and remaining coefficients are given in Appendix A. In  $f_3$ , the upper sign corresponds to  $p = 1$  and the lower sign corresponds to  $p = 3$ . For  $p = 1$ ,  $A_{\tilde{z}} > 0$  which gives northern halo and for  $p = 3$ ,  $A_{\tilde{z}} < 0$  which gives southern halo. This bifurcation of halo orbits gets manifested in the third order solution through the phase-angle relation

$$\psi = \phi + \frac{p\pi}{2}, \quad p = 1, 3$$

for values of  $A_{\tilde{x}}$  greater than a certain minimum value (Koon et al. (2011)).

For abolishing the secular term from the solution of last equation of system (2.21), we must have

$$v_6 \pm 2\omega_4\lambda^2 A_{\tilde{z}} = 0,\tag{2.22}$$

in which the upper sign corresponds to  $p = 1$  and the lower sign corresponds to  $p = 3$ .

Since the first two equations of the system (2.21) are coupled equations, for abolishing secular terms from their solution,

$$[v_4 + 2\lambda A_{\tilde{x}}\omega_4(nk - \lambda)] - k[v_5 + 2\lambda A_{\tilde{x}}\omega_4(\lambda k - n)] = 0$$

from which the value of  $\omega_4$  can be obtained as

$$\omega_4 = \frac{v_4 - kv_5}{2\lambda A_{\tilde{x}}[\lambda(k^2 + 1) - 2nk]}.\tag{2.23}$$

Applying the constraints (2.22) and (2.23) to system (2.21), the fifth order equations get converted to

$$\begin{aligned}\tilde{x}_5'' - 2n\tilde{y}_5' - (n^2 + 2C_2)\tilde{x}_5 &= k\beta_{11} \cos \tau_1 + \gamma_8 \cos 3\tau_1 + \gamma_9 \cos 5\tau_1, \\ \tilde{y}_5'' + 2n\tilde{x}_5' + (C_2 - n^2)\tilde{y}_5 &= \beta_{11} \sin \tau_1 + \beta_9 \sin 3\tau_1 + \beta_{10} \sin 5\tau_1, \\ \tilde{z}_5'' + \lambda^2\tilde{z}_5 &= \delta_8 \cos 3\tau_1 + \delta_9 \cos 5\tau_1, \quad p = 1, 3,\end{aligned}\tag{2.24}$$

where  $\beta_{11} = v_5 + 2\lambda A_{\tilde{x}}\omega_4(\lambda k - n)$ . The solution of the system (2.24) can be expressed as

$$\begin{aligned}\tilde{x}_5(\tau) &= \rho_{51} \cos 3\tau_1 + \rho_{52} \cos 5\tau_1, \\ \tilde{y}_5(\tau) &= \sigma_{51} \sin \tau_1 + \sigma_{52} \sin 3\tau_1 + \sigma_{53} \sin 5\tau_1, \\ \tilde{z}_5(\tau) &= k_{51} \cos 3\tau_1 + k_{52} \cos 5\tau_1.\end{aligned}\tag{2.25}$$

All coefficients appearing in above solution are given in Appendix A.

For acquiring the final approximation, the fifth order solution along with the first, second, third and fourth order solution is substituted into equations (2.19) and then  $\epsilon$  is removed from these solutions with the help of transformations  $A_{\tilde{x}} \rightarrow A_{\tilde{x}}/\epsilon$  and  $A_{\tilde{z}} \rightarrow A_{\tilde{z}}/\epsilon$ . Then system (2.19) gets transformed to

$$\begin{aligned}\tilde{x}(\tau) &= (\rho_{20} + \rho_{40}) - A_{\tilde{x}} \cos \tau_1 + (\rho_{21} - \rho_{22} + \rho_{41}) \cos 2\tau_1 \\ &\quad + (\rho_{31} + \rho_{51}) \cos 3\tau_1 + \rho_{42} \cos 4\tau_1 + \rho_{52} \cos 5\tau_1, \\ \tilde{y}(\tau) &= (kA_{\tilde{x}} + \sigma_{32} + \sigma_{51}) \sin \tau_1 + (\sigma_{21} + \sigma_{41} - \sigma_{22}) \sin 2\tau_1 \\ &\quad + (\sigma_{31} + \sigma_{52}) \sin 3\tau_1 + \sigma_{42} \sin 4\tau_1 + \sigma_{53} \sin 5\tau_1, \\ \tilde{z}(\tau) &= (-1)^{\frac{p-1}{2}} (A_{\tilde{z}} \cos \tau_1 + k_{21} \cos 2\tau_1 + k_{22} + k_{32} \cos 3\tau_1) \\ &\quad + k_{40} + k_{41} \cos 2\tau_1 + k_{42} \cos 4\tau_1 + k_{51} \cos 3\tau_1 + k_{52} \cos 5\tau_1, \quad p = 1, 3.\end{aligned}\tag{2.26}$$

Solutions (2.26) are used for generating the first guess of halo orbits. For this purpose, the Sun-Earth system with perturbations due to solar radiation pressure and oblateness of the Earth is considered. The state vectors of halo orbits around  $L_1$  calculated using the third, fourth and fifth order analytic solutions are given in Tables 2.1, 2.2 and 2.3, respectively, for different values of  $q_1$  and  $A_2$ . For getting this initial guess,  $A_{\tilde{z}} = 1.25 \times 10^5$  km is considered. The corresponding value of  $A_{\tilde{x}}$  can be obtained from the amplitude constraint relation (Richardson (1980)). In Tables 2.1-2.3,  $A_2 = 0$  shows oblateness of the Earth is not considered,  $A_2 = 2.42405 \times 10^{-12}$  is the actual oblateness of the Earth and  $q_1 = 1$  denotes that perturbation due to solar radiation pressure is not considered.

In Fig. 2.1, halo orbits around  $L_1$  obtained using the third, fourth and fifth order Lindstedt-Poincaré method are plotted in blue, green and red colour, respectively. The  $xy$ ,  $xz$  and  $yz$  projections of these orbits are given in Figs. 2.2, 2.3 and 2.4, respectively. The separation between the third and fourth order analytic solution is 4784.44 km and the separation between the fourth and fifth order analytic solution is 1951.61 km which indicates that the separation between the successive solutions decreases as the order of solution increases. This can be observed from Figs. 2.1-2.4 as well.

TABLE 2.1: Initial guess from the third order analytical solution around  $L_1$  in the Sun-Earth system

$q_1$	$A_2$	Initial guess					
		$x(\times 10^8)$ (km)	$y$	$z(\times 10^5)$ (km)	$\dot{x}$	$\dot{y}$ (km/s)	$\dot{z}$
0.99	0	1.482238677364	0	-1.133909207584	0	-0.9199293912363	0
0.979	$2.42405 \times 10^{-12}$	1.480573596221	0	-1.136492217736	0	-0.8539269651719	0
1	$2.42405 \times 10^{-12}$	1.483432365376	0	-1.139593655307	0	-0.9691542403827	0
1	0	1.483432365530	0	-1.139593655225	0	-0.9691542409496	0

TABLE 2.2: Initial guess from the fourth order analytical solution around  $L_1$  in the Sun-Earth system

$q_1$	$A_2$	Initial guess					
		$x(\times 10^8)$ (km)	$y$	$z(\times 10^5)$ (km)	$\dot{x}$	$\dot{y}$ (km/s)	$\dot{z}$
0.99	0	1.482210682231	0	-1.162260965275	0	-0.9201578350097	0
0.979	$2.42405 \times 10^{-12}$	1.480532643379	0	-1.168284121572	0	-0.8535828234300	0
1	$2.42405 \times 10^{-12}$	1.483416559976	0	-1.162808064038	0	-0.9697930252479	0
1	0	1.483416560131	0	-1.162808063984	0	-0.9697930258232	0

Using the same value of  $A_z$ , initial guess for halo orbits around  $L_2$  is also computed using the third, fourth and fifth order analytic solutions. The initial state vectors of these halo orbits corresponding to various values of  $q_1$  and  $A_2$  are given in Tables 2.4-2.6.

TABLE 2.3: Initial guess from the fifth order analytical solution around  $L_1$  in the Sun-Earth system

$q_1$	$A_2$	Initial guess					
		$x(\times 10^8)$ (km)	$y$	$z(\times 10^5)$ (km)	$\dot{x}$	$\dot{y}$ (km/s)	$\dot{z}$
0.99	0	1.482214355512	0	-1.163220390129	0	-0.9282323898148	0
0.979	$2.42405 \times 10^{-12}$	1.480538040599	0	-1.168636401854	0	-0.8662066148866	0
1	$2.42405 \times 10^{-12}$	1.483418634032	0	-1.169496960363	0	-0.8597224569674	0
1	0	1.483418634187	0	-1.163537425035	0	-0.9794676169398	0

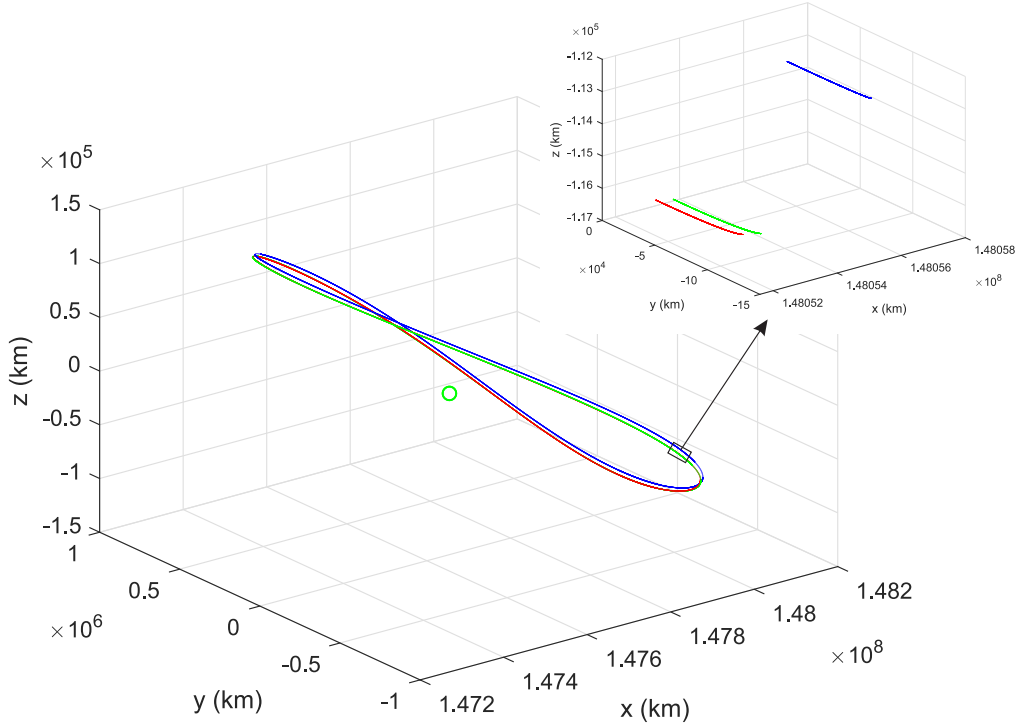


FIGURE 2.1: The third, fourth and fifth order Analytic solutions around  $L_1$  with  $q_1 = 0.979$  and  $A_2 = 2.424052106866 \times 10^{-12}$

Halo orbits around  $L_2$  for  $q_1 = 0.979$  and  $A_2 = 2.424052106866 \times 10^{-12}$  obtained using the state vectors given in Tables 2.4-2.6 are plotted in Fig. 2.5. The  $xy, xz$  and  $yz$  projections of these orbits are given in Figs. 2.6, 2.7 and 2.8, respectively. In Figs. 2.5-2.8, orbits in blue, red and green corresponds to the third, fourth and fifth order solution, respectively. In this case also, the separation between the fifth order and fourth order solution is less than the separation between the fourth order and the third order solution.

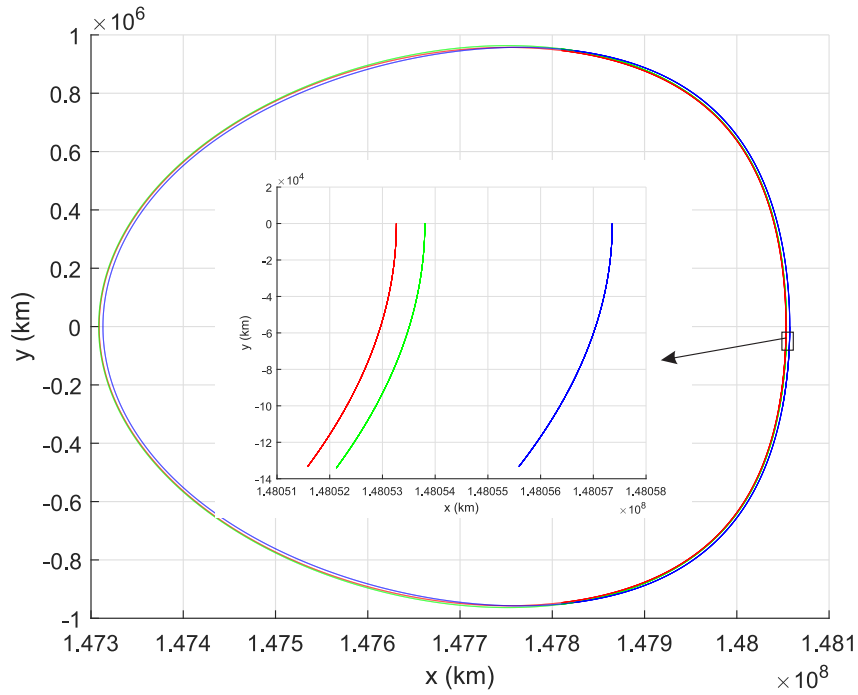


FIGURE 2.2:  $xy$  projections of the third, fourth and fifth order analytic solutions around  $L_1$  with  $q_1 = 0.979$  and  $A_2 = 2.424052106866 \times 10^{-12}$

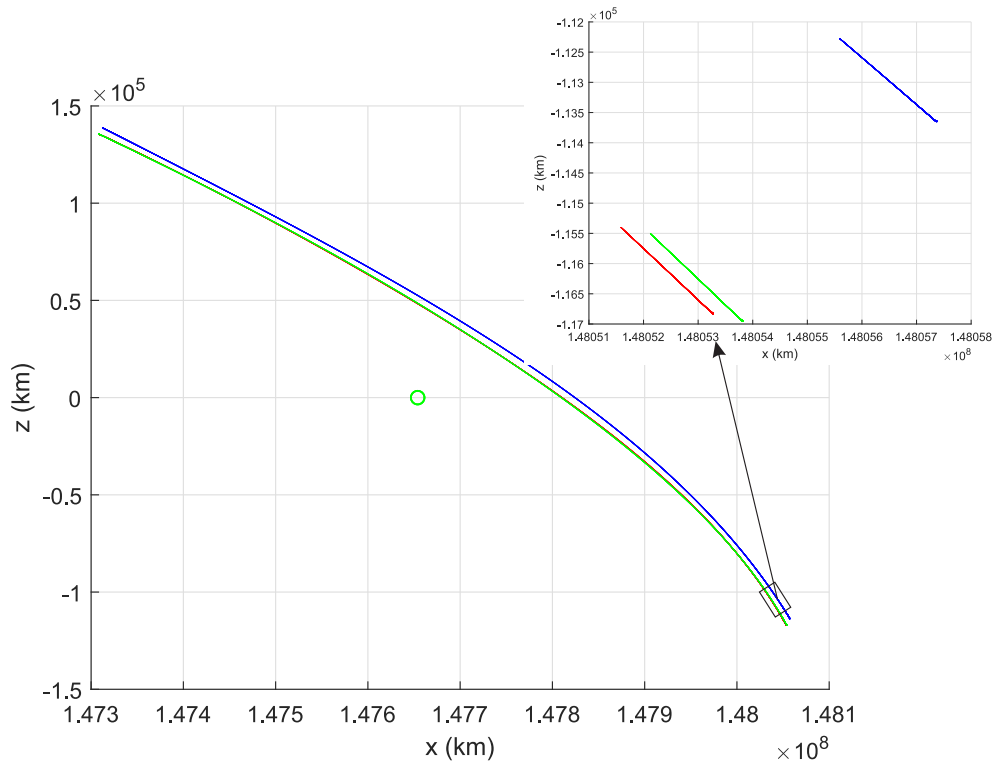


FIGURE 2.3:  $xz$  projections of the third, fourth and fifth order analytic solutions around  $L_1$  with  $q_1 = 0.979$  and  $A_2 = 2.424052106866 \times 10^{-12}$

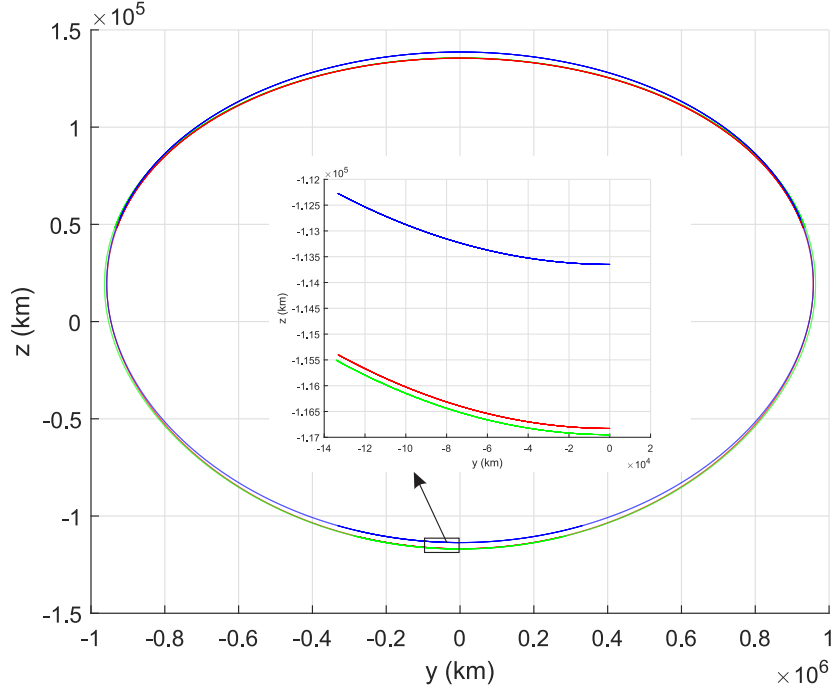


FIGURE 2.4:  $yz$  projections of the third, fourth and fifth order analytic solutions around  $L_1$  with  $q_1 = 0.979$  and  $A_2 = 2.424052106866 \times 10^{-12}$

## 2.2.2 Numerical solution of halo orbits around $L_1$ and $L_2$

Analytic solutions computed using Lindstedt-Poincaré method are revised by applying Differential Correction (DC) method. The third, fourth and fifth order analytic solutions are inserted as initial guess of the solution in DC method. State vectors of halo orbits around  $L_1$  computed using DC method are given in Tables 2.7-2.9. Halo orbits obtained using these solutions are plotted in Fig. 2.9 and their  $xy$ ,  $xz$  and  $yz$  projections are given in Figs. 2.10, 2.11 and 2.12, respectively. Orbits in cyan, magenta and black colours correspond to the third, fourth and fifth order solution, respectively. From Figs. 2.9-2.12, it can be observed that the separation between the solution decreases as the order of solution increases. The separation between the fifth and the fourth order solution is 122.33 km and the separation between the fourth and the third order solution is 3205.85 km. In Table 2.13, separation between the third, fourth and fifth order analytic and numerical solutions for different values of  $q_1$  and  $A_2$  are given.

State vectors of halo orbits around  $L_2$  computed using DC method are given in Tables 2.10-2.12. Halo orbits obtained using these solutions are plotted in Fig. 2.13 and their  $xy$ ,  $xz$  and  $yz$  projections are given in Figs. 2.14, 2.15 and 2.16, respectively. Orbits in cyan, magenta and black colours correspond to the third, fourth and fifth

TABLE 2.4: Initial guess from the third order analytical solution around  $L_2$  in the Sun-Earth system

$q_1$	$A_2$	Initial guess					
		$x(\times 10^8)$ (km)	$y$	$z(\times 10^5)$ (km)	$\dot{x}$	$\dot{y}$ (km/s)	$\dot{z}$
0.99	0	1.510804811691	0	-1.371615994153	0	-0.9281901534292	0
0.979	$2.42405 \times 10^{-12}$	1.509115808560	0	-1.355088561477	0	-0.9614392217686	0
1	$2.42405 \times 10^{-12}$	1.512799359163	0	-1.385564724333	0	-0.8912931779191	0
1	0	1.512799358962	0	-1.385564724361	0	-0.8912931782033	0

TABLE 2.5: Initial guess from the fourth order analytical solution around  $L_2$  in the Sun-Earth system

$q_1$	$A_2$	Initial guess					
		$x(\times 10^8)$ (km)	$y$	$z(\times 10^5)$ (km)	$\dot{x}$	$\dot{y}$ (km/s)	$\dot{z}$
0.99	0	1.510811465779	0	-1.352312961004	0	-0.9272507788787	0
0.979	$2.42405 \times 10^{-12}$	1.509115968500	0	-1.340918416255	0	-0.9604076673270	0
1	$2.42405 \times 10^{-12}$	1.512815720807	0	-1.360667556390	0	-0.8905902892661	0
1	0	1.512815720606	0	-1.360667556405	0	-0.8905902895425	0

TABLE 2.6: Initial guess from the fifth order analytical solution around  $L_2$  in the Sun-Earth system

$q_1$	$A_2$	Initial guess					
		$x(\times 10^8)$ (km)	$y$	$z(\times 10^5)$ (km)	$\dot{x}$	$\dot{y}$ (km/s)	$\dot{z}$
0.99	0	1.510812566524	0	-1.163220390129	0	-0.9387394164807	0
0.979	$2.42405 \times 10^{-12}$	1.509116373712	0	-1.341334996462	0	-0.9739509441934	0
1	$2.42405 \times 10^{-12}$	1.512818025419	0	-1.361471747499	0	-0.9005070159124	0
1	0	1.512818025218	0	-1.361471747514	0	-0.9005070163730	0

order solution, respectively. From Figs. 2.13-2.16, it can be observed that the separation between the solution decreases as the order of solution increases. The separation

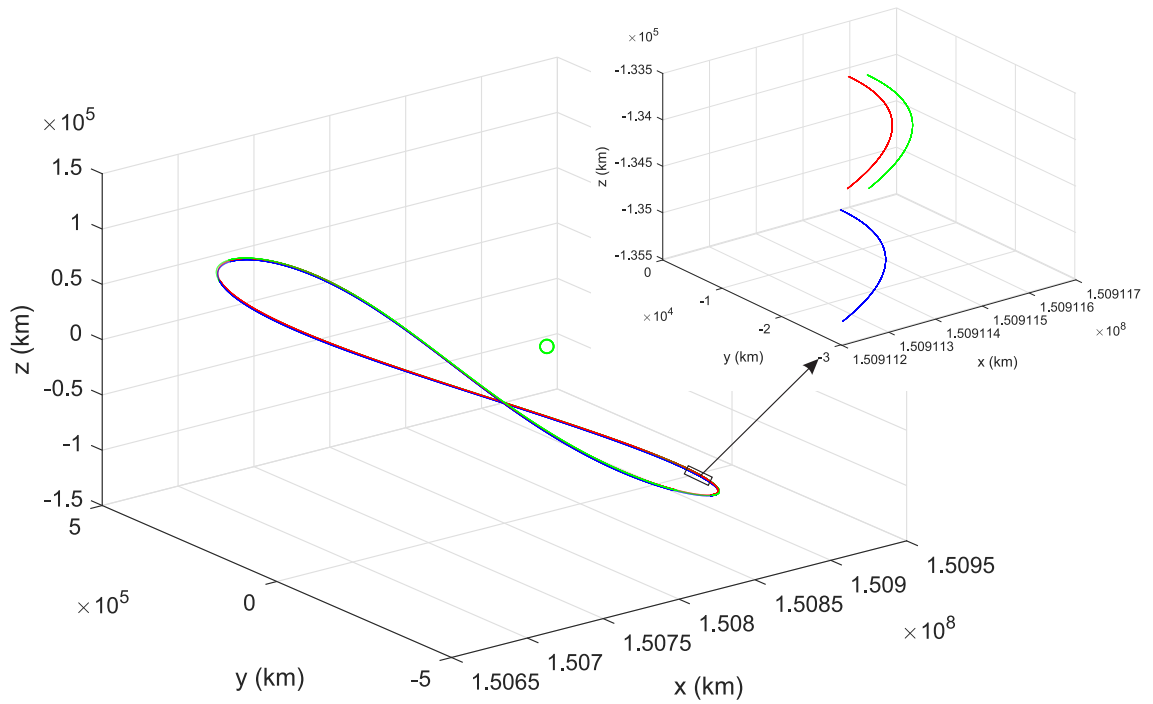


FIGURE 2.5: The third, fourth and fifth order Analytic solutions around  $L_2$  with  $q_1 = 0.979$  and  $A_2 = 2.424052106866 \times 10^{-12}$

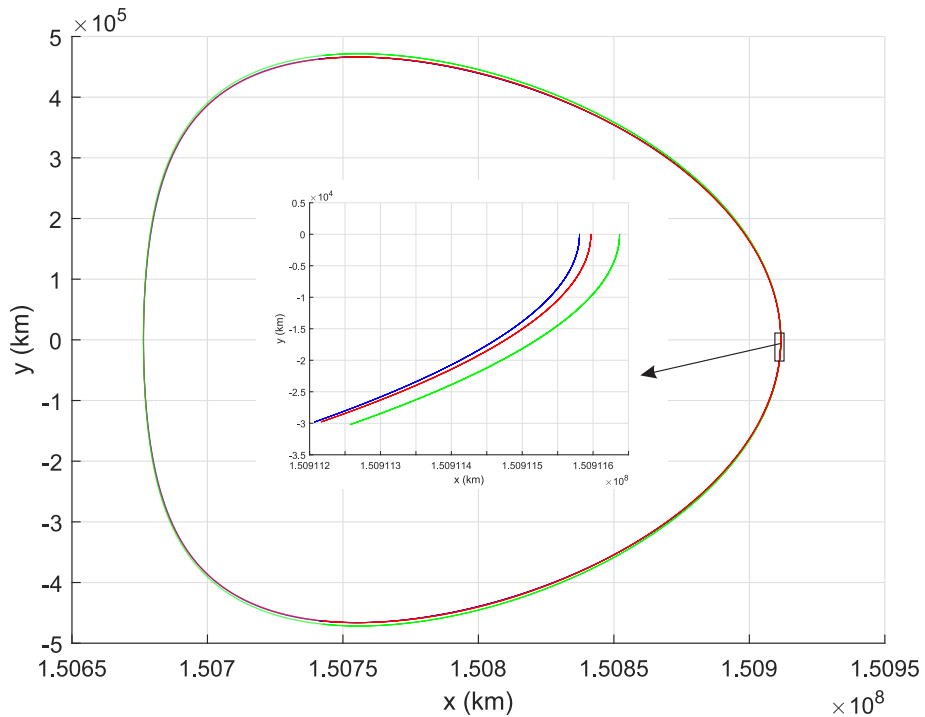


FIGURE 2.6:  $xy$  projections of the third, fourth and fifth order analytic solutions around  $L_2$  with  $q_1 = 0.979$  and  $A_2 = 2.424052106866 \times 10^{-12}$

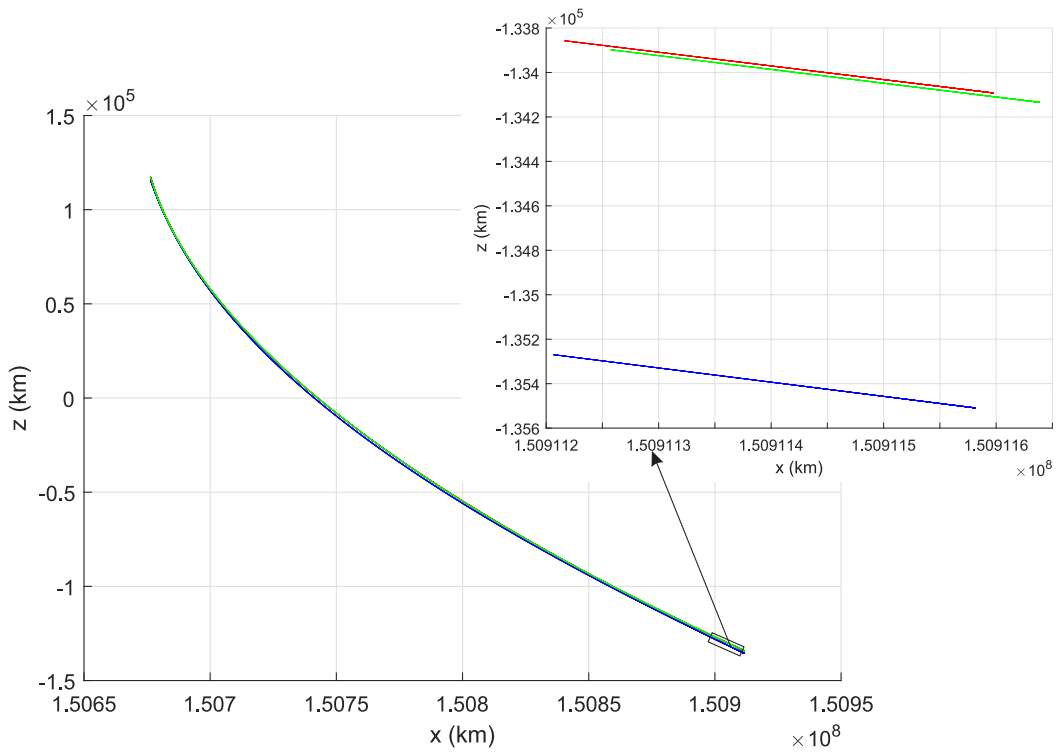


FIGURE 2.7:  $xz$  projections of the third, fourth and fifth order analytic solutions around  $L_2$  with  $q_1 = 0.979$  and  $A_2 = 2.424052106866 \times 10^{-12}$

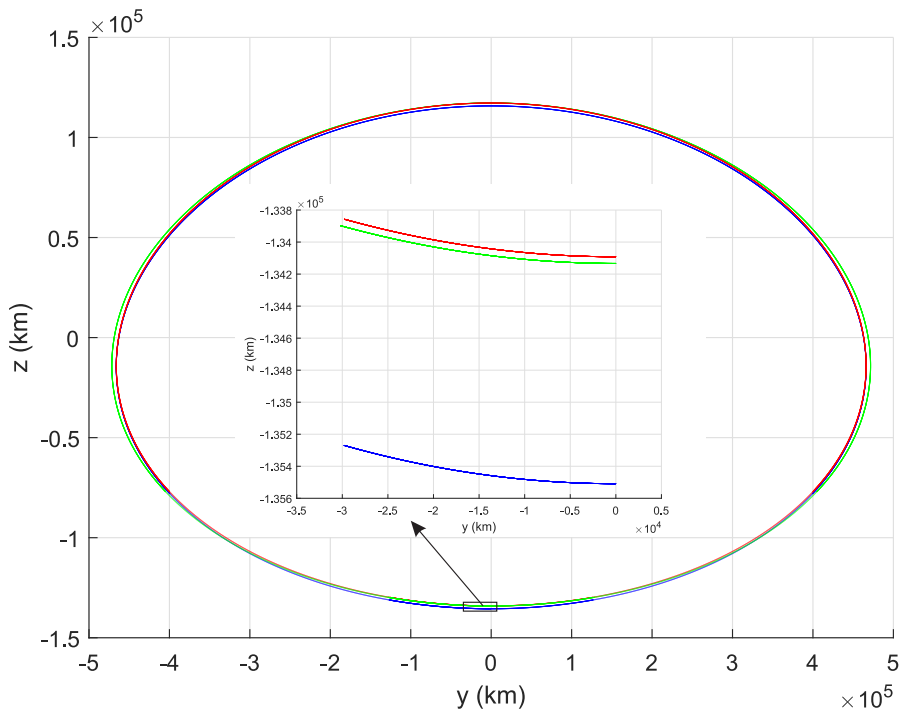


FIGURE 2.8:  $yz$  projections of the third, fourth and fifth order analytic solutions around  $L_2$  with  $q_1 = 0.979$  and  $A_2 = 2.424052106866 \times 10^{-12}$

between the fifth and the fourth order solution is 41.71 km and the separation between the fourth and the third order solution is 1418.93 km. In Table 2.14, separation between the third, fourth and fifth order analytical and numerical solutions for different values of  $q_1$  and  $A_2$  are given.

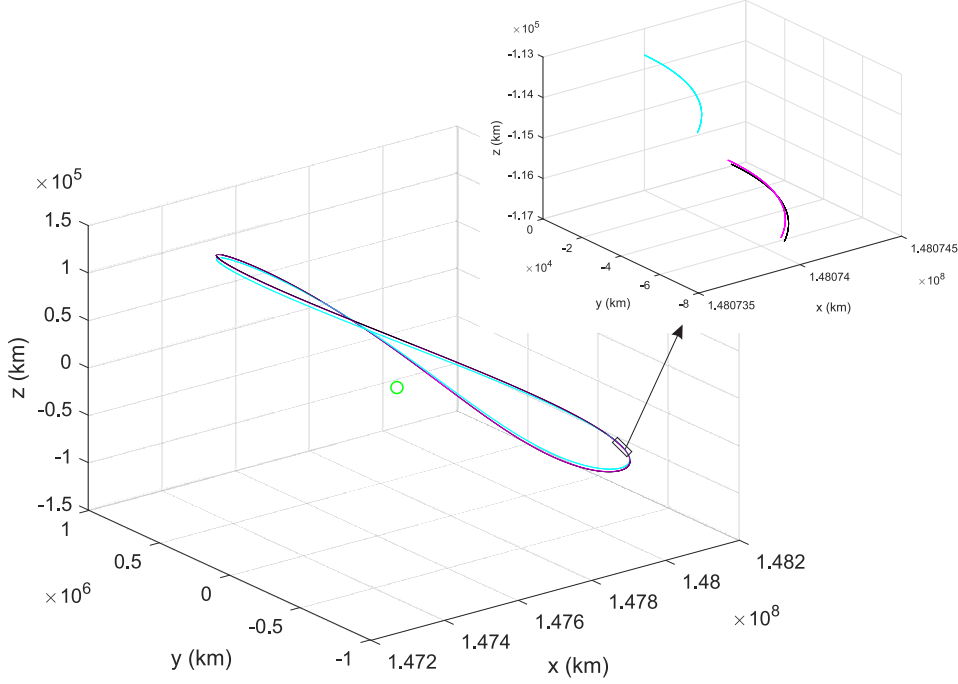


FIGURE 2.9: The third, fourth and fifth order Numerical solutions around  $L_1$  with  $q_1 = 0.979$  and  $A_2 = 2.424052106866 \times 10^{-12}$

## 2.3 Results and Discussion

Circular Restricted Three Body Problem (CRTBP) is considered with both the primaries radiating as well as oblate spheroids. Effects of these perturbations on locations of collinear Lagrangian points and parameters of halo orbits are analyzed. For analyzing deviations in locations and parameters of halo orbits around  $L_1$  and  $L_2$  due to radiation ( $q_2$ ) of the second primary ( $P_2$ ) and oblateness ( $A_1$ ) of the first primary ( $P_1$ ), mass ratio  $\mu = 0.004$  and  $A_{\tilde{z}} = 4.881785271574502 \times 10^{-4}/\gamma$  are considered. These values are selected randomly. For studying the effects of perturbing forces on location of  $L_3$  and halo orbits around it, the Sun-Earth system with the Sun as a source of radiation and the Earth as an oblate spheroid is considered. Here,  $A_{\tilde{x}} = 0.045$ , a random value, is taken for getting parameters of halo orbits.

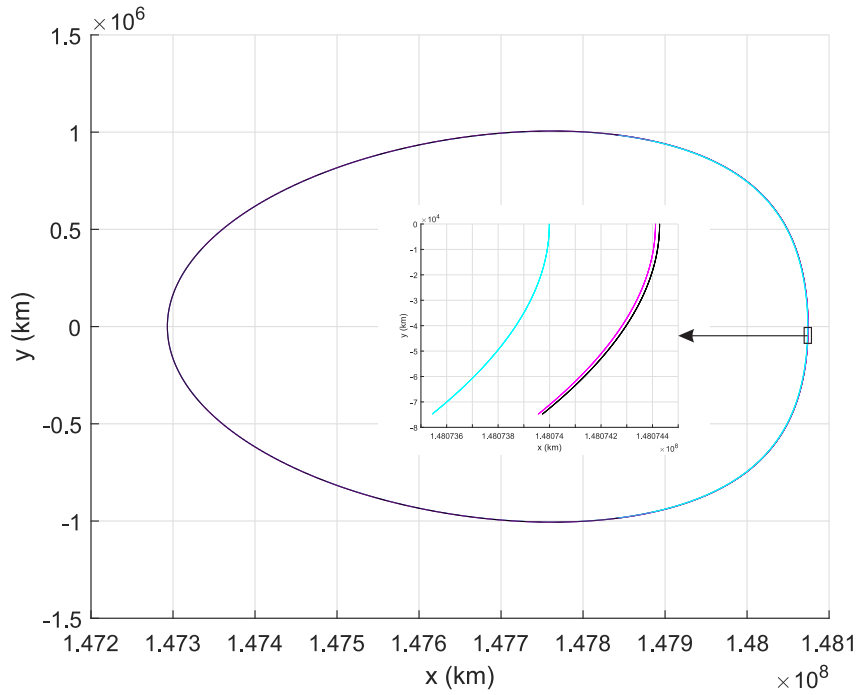


FIGURE 2.10:  $xy$  projections of the third, fourth and fifth order numerical solutions around  $L_1$  with  $q_1 = 0.979$  and  $A_2 = 2.424052106866 \times 10^{-12}$

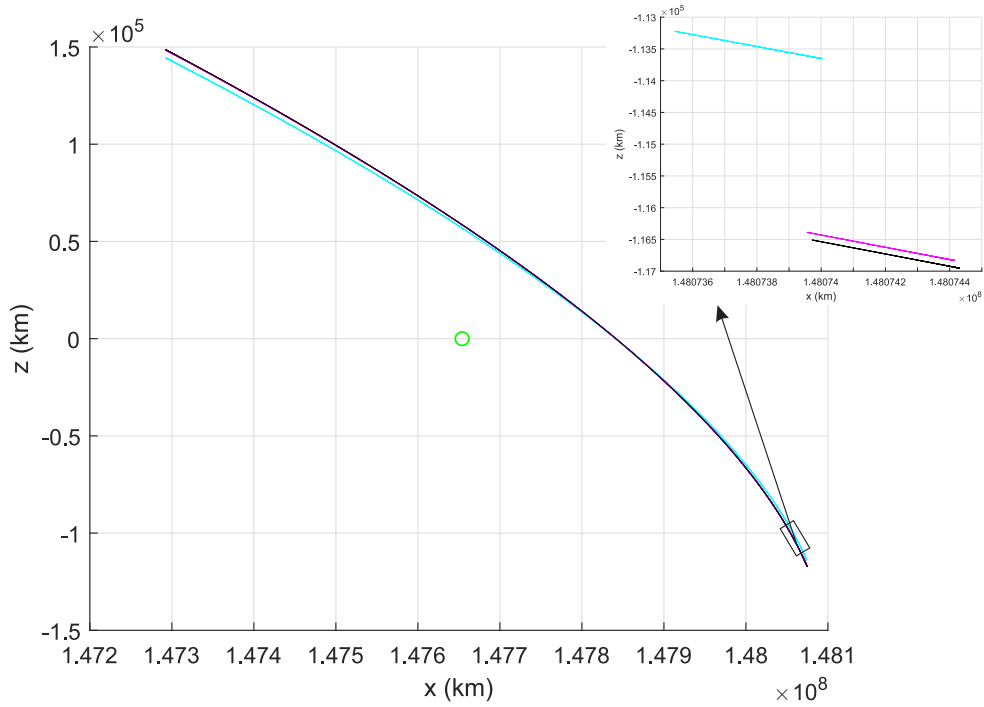


FIGURE 2.11:  $xz$  projections of the third, fourth and fifth order numerical solutions around  $L_1$  with  $q_1 = 0.979$  and  $A_2 = 2.424052106866 \times 10^{-12}$

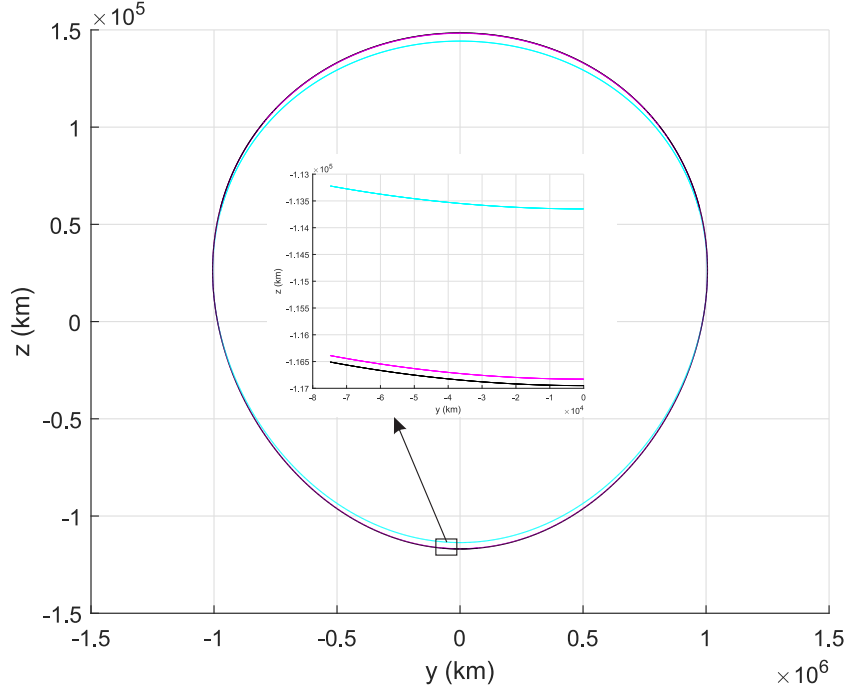


FIGURE 2.12:  $yz$  projections of the third, fourth and fifth order numerical solutions around  $L_1$  with  $q_1 = 0.979$  and  $A_2 = 2.424052106866 \times 10^{-12}$

### 2.3.1 Effects of radiation pressure

For analyzing the effects  $q_2$  on parameters of halo orbits, different values of  $q_2$  in the interval  $[0.89, 1]$  are considered. The change in locations of  $L_1$  and  $L_2$  due to radiation of  $P_1$  is shown in Fig. 2.17. As radiation of  $P_1$  increases,  $L_1$  moves away from  $P_1$  and goes closer to  $P_2$  (Fig. 2.17(A)). Lagrangian point  $L_2$  shifts towards  $P_2$  and hence towards  $P_1$  as well due to increase in radiation of  $P_1$  (Fig. 2.17(B)). Variation in period of halo orbits around  $L_1$  and  $L_2$  are given in Fig, 2.18. As radiation increases, period of orbits around  $L_1$  increases (Fig. 2.18(A)) whereas period of orbits around  $L_2$  decreases (2.18(B)). In Fig. 2.19, variation in size of orbits around  $L_1$  and  $L_2$  due to increase in radiation pressure of  $P_1$  is shown. In Fig. 2.19(A), halo orbits around  $L_1$  for  $q_2 = 0.99, 0.75, 0.50$  and  $0.25$  are plotted in blue, red, green and magenta colours, respectively. The  $xy$  and  $yz$  projections of these orbits are given in Figs. 2.19(C) and 2.19(E), respectively. Similarly, halo orbits around  $L_2$  for above listed four values of  $q_2$  are plotted in Fig. 2.19(B) and their  $xy$  and  $yz$  projections are given in Figs. 2.19(D) and 2.19(F), respectively. In these figures also, blue, red, green and magenta coloured orbits correspond to  $q_2 = 0.99, 0.75, 0.50$  and  $0.25$ , respectively.

The values of  $\gamma$ , location of Lagrangian points,  $\Delta, \tau$  and coefficients  $C_i$  ( $i = 2, 3, 4, 5, 6$ )

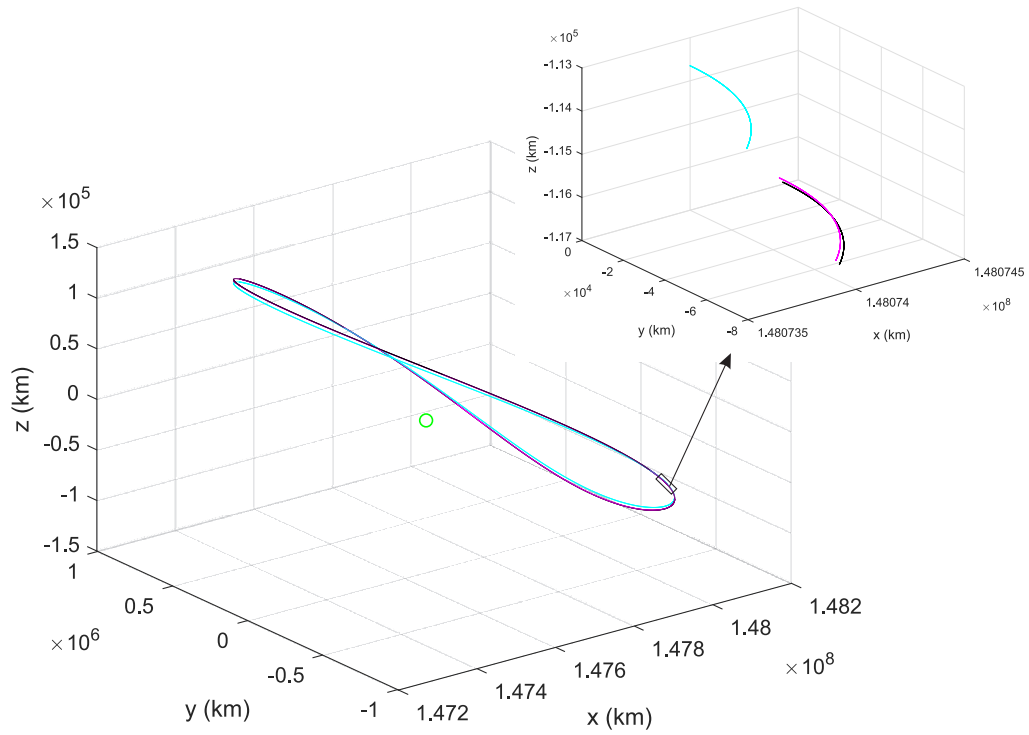


FIGURE 2.13: The third, fourth and fifth order Numerical solutions around  $L_2$  with  $q_1 = 0.979$  and  $A_2 = 2.424052106866 \times 10^{-12}$

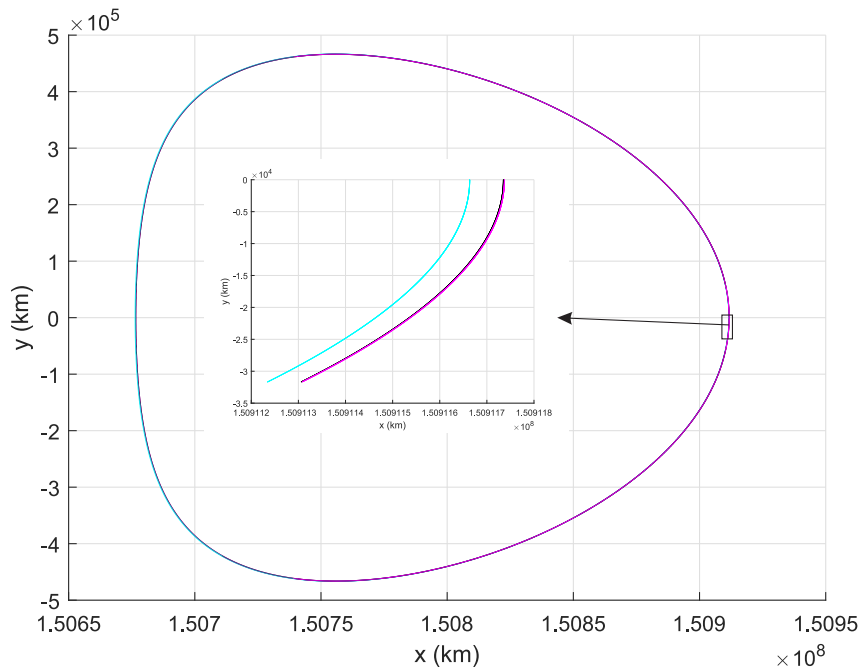


FIGURE 2.14:  $xy$  projections of the third, fourth and fifth order numerical solutions around  $L_2$  with  $q_1 = 0.979$  and  $A_2 = 2.424052106866 \times 10^{-12}$

for  $q_2 = 0.99, 0.75, 0.50$  and  $0.25$  for halo orbits around  $L_1$  and  $L_2$  are given in Tables 2.15 and 2.16, respectively. Here, for all computations and plotting of orbits,

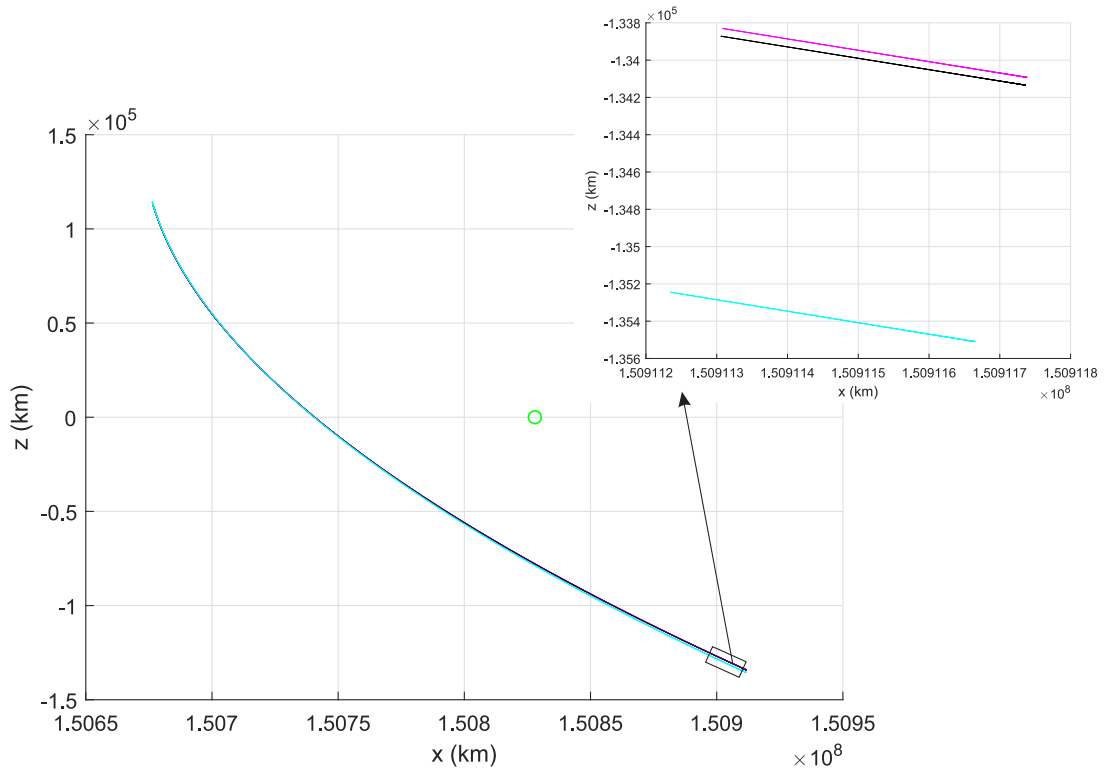


FIGURE 2.15:  $xz$  projections of the third, fourth and fifth order numerical solutions around  $L_2$  with  $q_1 = 0.979$  and  $A_2 = 2.424052106866 \times 10^{-12}$

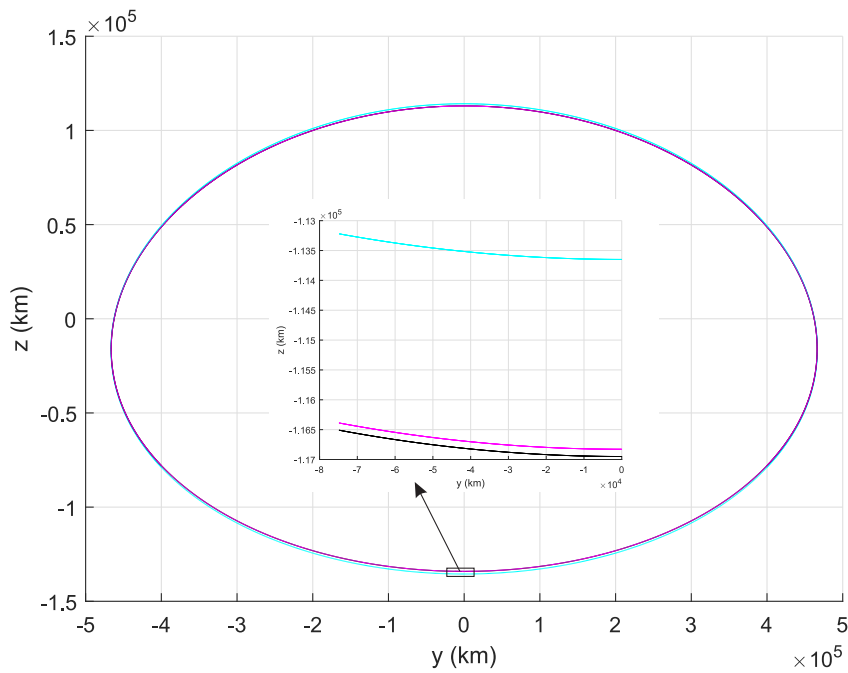
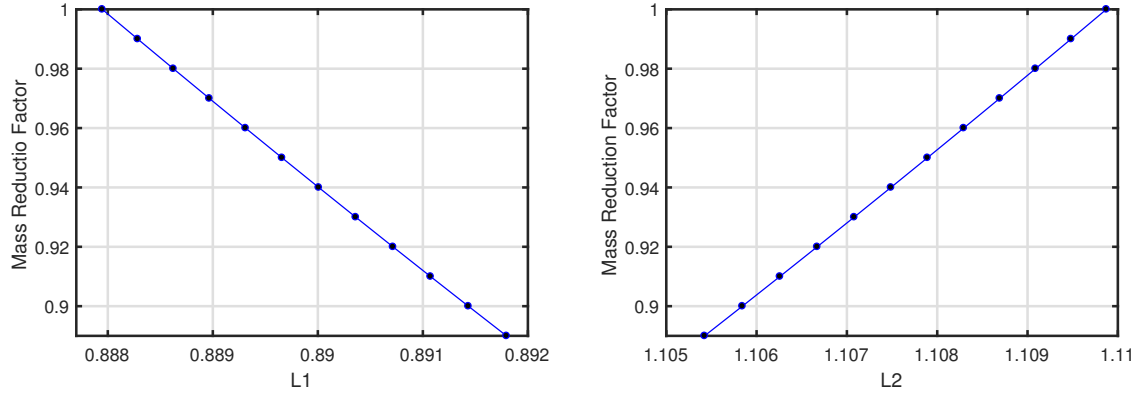


FIGURE 2.16:  $yz$  projections of the third, fourth and fifth order numerical solutions around  $L_2$  with  $q_1 = 0.979$  and  $A_2 = 2.424052106866 \times 10^{-12}$



(A) Change in position against variation in  $q_2$  around  $L_1$  (B) Change in position against variation in  $q_2$  around  $L_2$

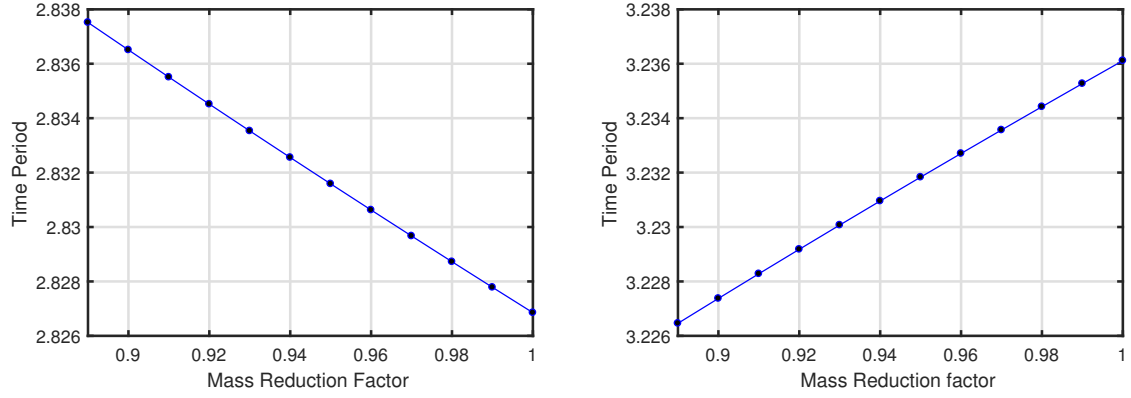
FIGURE 2.17: Effect of radiation pressure on the position of halo orbits around  $L_1$  and  $L_2$

$A_1 = A_2 = 0.0002$  and  $q_1 = 0.99$  are considered.

The Sun-Earth system is considered to study the effects of solar radiation pressure and oblateness of the Earth on parameters of halo orbits around  $L_3$ . Fig. 2.20 shows halo orbits around  $L_3$  for four different values of  $q_1$ . Orbits in blue, red, green and magenta correspond to  $q_1 = 1.00, 0.95, 0.90$  and  $0.85$ , respectively. Here,  $q_2 = 1$  and  $A_1 = A_2 = 0$  are considered for plotting orbits. It can be observed from Fig. 2.20 that as solar radiation pressure increases, halo orbits around  $L_3$  shrink. In Table 2.17, parameters of these orbits for different values of  $q_1$  and  $A_2$  are given. It can be observed that halo orbits around  $L_3$  shift towards the Sun as radiation pressure increases. Also, due to solar radiation, period of orbits decreases whereas the  $\tilde{z}$  amplitude,  $A_{\tilde{z}}$ , increases (Table 2.17).

### 2.3.2 Effects of oblateness

To analyze changes in locations and parameters of halo orbits around  $L_1$  and  $L_2$  due to oblateness of the first primary ( $P_1$ ), different values of  $A_1$  in the range  $[0.066, 1]$  are considered. In Fig. 2.21, orbits corresponding to  $A_1 = 0.0002, 0.0500, 0.0999$  and  $0.1500$  around  $L_1$  and  $L_2$  are plotted in blue, red, green and magenta colours, with  $A_2 = 0.0002, q_1 = 0.99$  and  $q_2 = 0.99$ . Locations of Lagrangian points and parameters of these orbits are given Tables 2.18 and 2.19. It can be noticed that as the value of  $A_1$  increases, orbits around  $L_1$  and  $L_2$  both expand. Fig. 2.22(A) shows that as oblateness of the first primary increases, halo orbits around  $L_1$  move towards the second primary and halo orbits around  $L_2$  move towards the first primary (Fig. 2.22(B)). Variation



(A) Change in period against variation in  $q_2$  around  $L_1$  (B) Change in period against variation in  $q_2$  around  $L_2$

FIGURE 2.18: Effect of radiation pressure on the period of halo orbits around  $L_1$  and  $L_2$

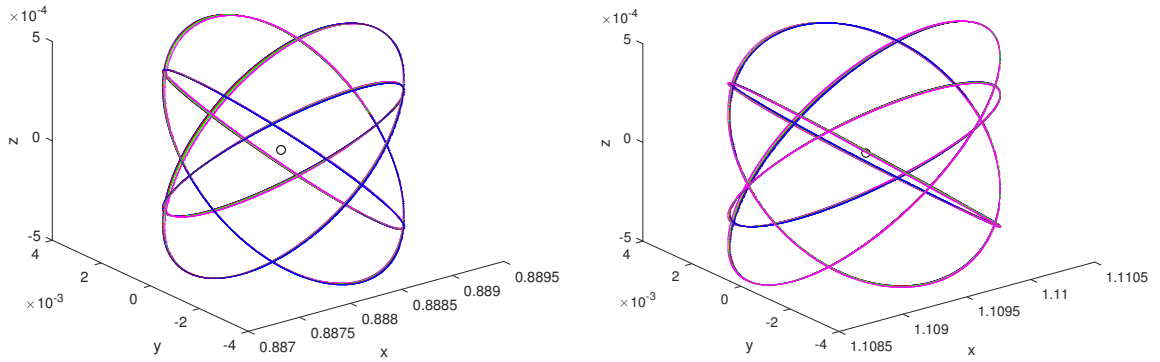
in period of these orbits around  $L_1$  and  $L_2$  are shown in Fig. 2.23. As value of  $A_1$  increases, period of orbits around  $L_1$  and  $L_2$  both decrease (Figs. 2.23(A), 2.23(B)).

As an application, this model has been applied to the Earth-Moon system with  $A_{\tilde{z}} = 0.338933597544932$  in dimensionless system for observing effects of Earth's oblateness on parameters of halo orbits. Halo orbits around  $L_1$  and  $L_2$  in the Earth-Moon system are shown in Figs. 2.24 and 2.25, respectively. In both the figures, blue orbit shows that oblateness of the Earth is neglected and red orbit corresponds to  $A_1 = 3.6715 \times 10^{-7}$ , the actual oblateness of the Earth. In this case, mass factor is  $\mu = 0.0122$  and  $q_1 = q_2 = 1, A_2 = 0$ . The values of masses and radii of the Earth and the Moon are taken from NASA Fact Sheets (<https://nssdc.gsfc.nasa.gov/planetary/factsheet/earthfact.html>, <https://nssdc.gsfc.nasa.gov/planetary/factsheet/moonfact.html>).

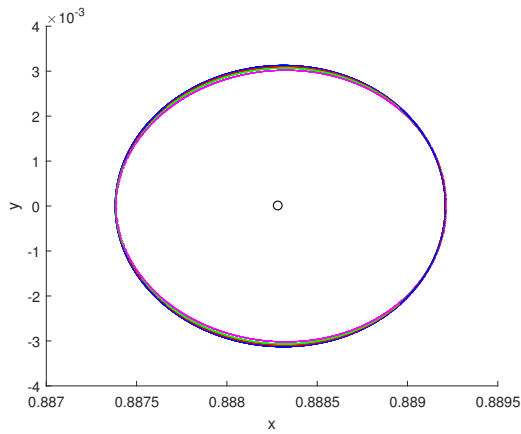
From Table 2.17, it can be observed that due to oblateness of the second primary ( $P_2$ ), halo orbits around  $L_3$  shift towards the Sun and period as well as  $\tilde{z}$  amplitude decreases.

## 2.4 Conclusions

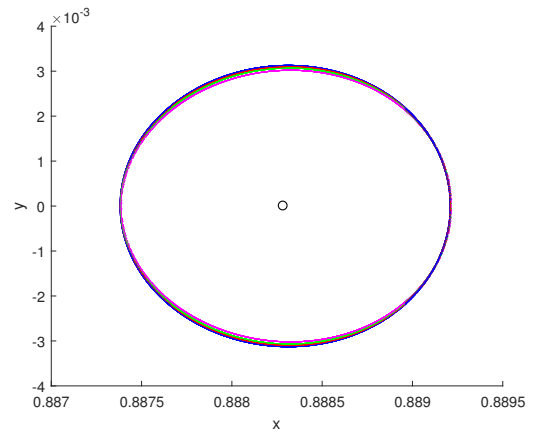
In this chapter, Circular Restricted Three Body Problem (CRTBP) with both the primaries radiating as well as oblate are considered and fifth order analytical solution for getting an initial guess of halo orbits around  $L_1, L_2$  and  $L_3$  is obtained using Lindstedt-Poincaré method. Also, variations in locations and parameters of halo orbits around collinear Lagrangian points due to oblateness and radiation of primaries are analyzed.



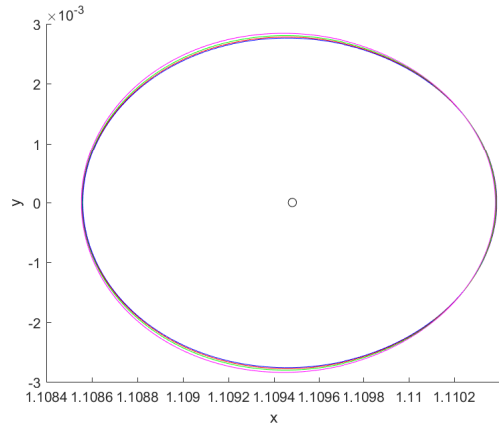
(A) Change in size against variation in  $q_2$  around  $L_1$  (B) Change in size against variation in  $q_2$  around  $L_2$



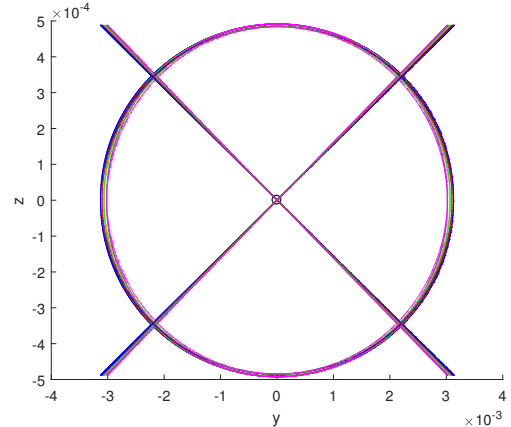
(C) xy projection of Fig. 2.19(A)



(D) xy projection of Fig. 2.19(B)



(E) yz projection of Fig. 2.19(A)



(F) yz projection of Fig. 2.19(B)

FIGURE 2.19: Effect of radiation pressure on the size of halo orbits around  $L_1$  and  $L_2$

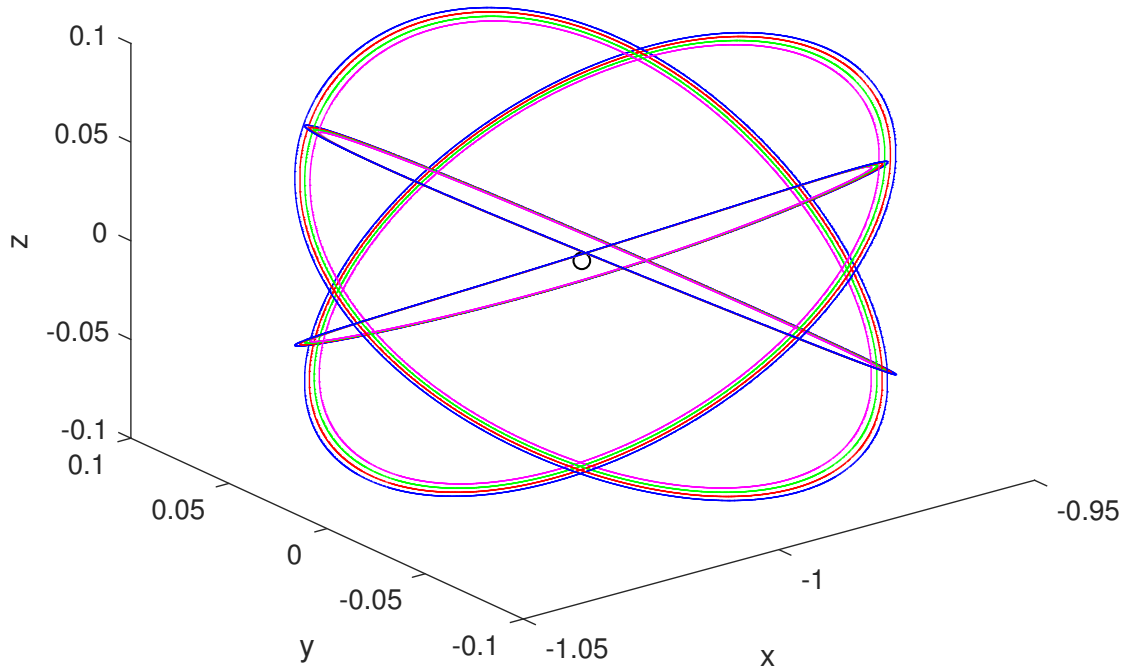
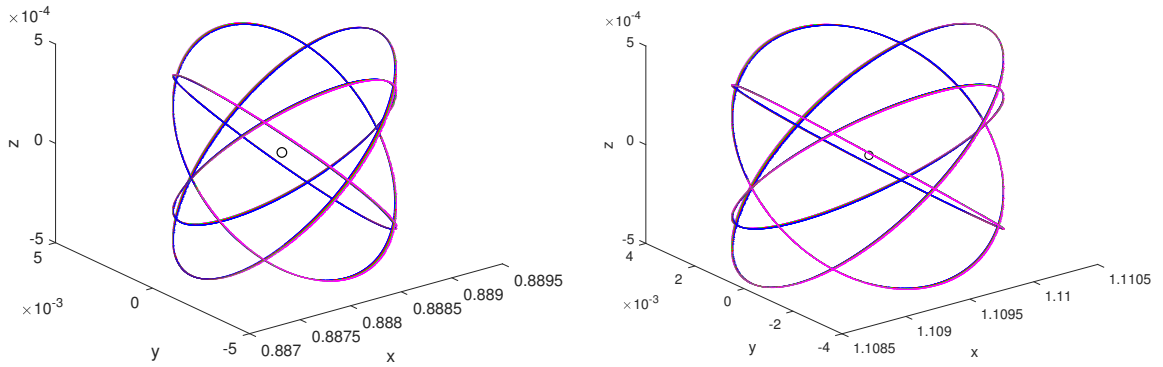


FIGURE 2.20: Sun-Earth system

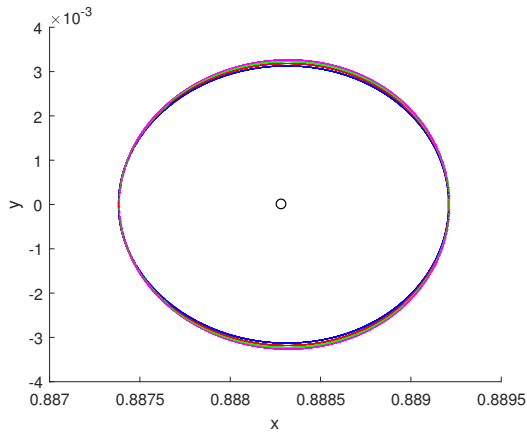
It is found that as the radiation pressure of the second primary increases, halo orbits around  $L_1$  contract, shift towards the second primary and their period increase whereas halo orbits around  $L_2$  elongate, move towards the second primary and their periods decrease. Due to increase in the radiation of the more massive primary, halo orbits around  $L_3$  shift towards the more massive primary  $P_1$  and their periods decrease.

The effects of oblateness of the first primary on parameters of halo orbits around  $L_1$  and  $L_2$  are analyzed. Due to oblateness of the first primary, orbits around  $L_1$  and  $L_2$  both elongate, shift towards the second primary and their periods decrease. This model is applied to the Earth-Moon system. Observations show that due to oblateness of the Earth, halo orbits around  $L_1$  and  $L_2$  elongate and go nearer to the Moon. Further, period of these orbits decrease. Due to oblateness of the second primary, halo orbits around  $L_3$  move towards the first primary and their periods decrease.

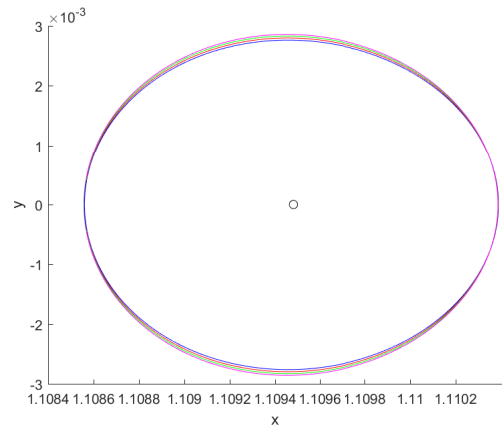
It has been observed that as the order of solution increases, the separation between consecutive orbits decreases, which indicates the convergence to the actual solution.



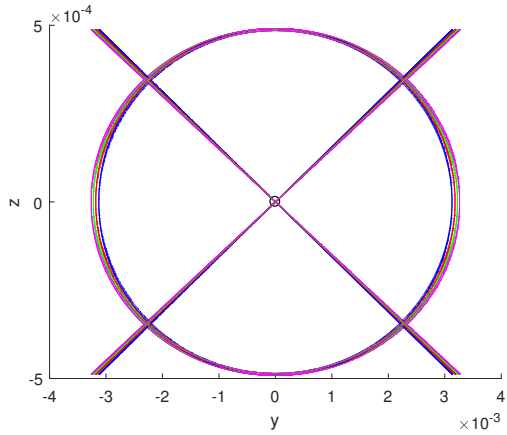
(A) Change in the size of orbits against variation (B) Change in the size of orbits against variation in  $A_1$  around  $L_1$  in  $A_1$  around  $L_2$



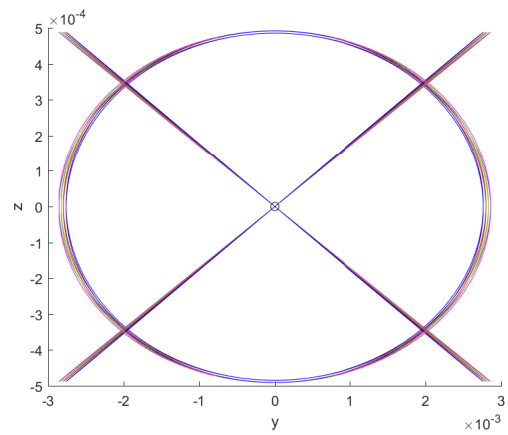
(C) xy projection of Fig. 2.21(A)



(D) xy projection of Fig. 2.21(B)

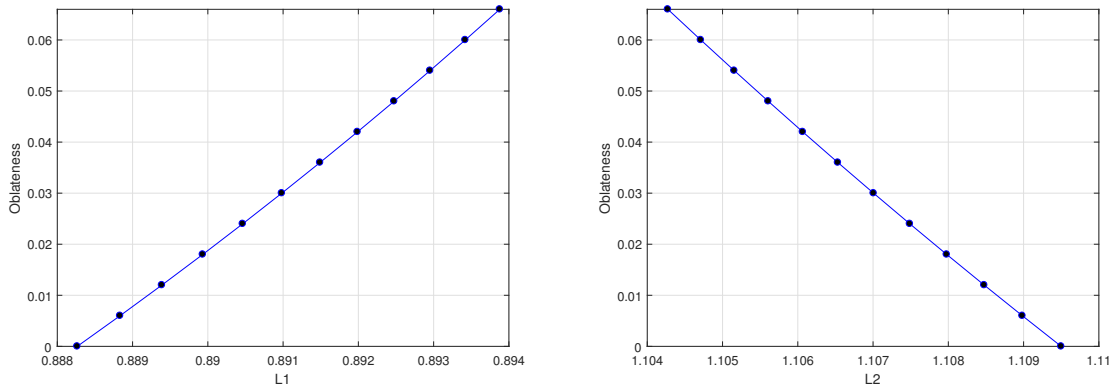


(E) yz projection of Fig. 2.21(A)



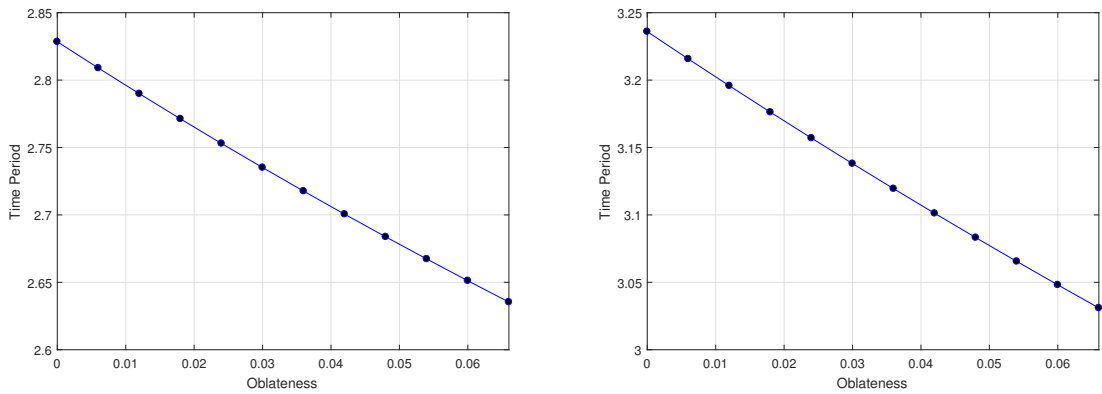
(F) yz projection of Fig. 2.21(B)

FIGURE 2.21: Effect of oblateness on the size of halo orbits around  $L_1$  and  $L_2$



(A) Change in the position against variation in  $A_1$  around  $L_1$  (B) Change in the position against variation in  $A_1$  around  $L_2$

FIGURE 2.22: Effect of oblateness on the position of  $L_1$  and  $L_2$



(A) Change in the period against variation in  $A_1$  around  $L_1$  (B) Change in the period against variation in  $A_1$  around  $L_2$

FIGURE 2.23: Effect of oblateness on the period of halo orbits around  $L_1$  and  $L_2$

So, it can be concluded that use of fifth order solution as an initial guess in differential correction method provides more accurate solution than the fourth or third order solution.

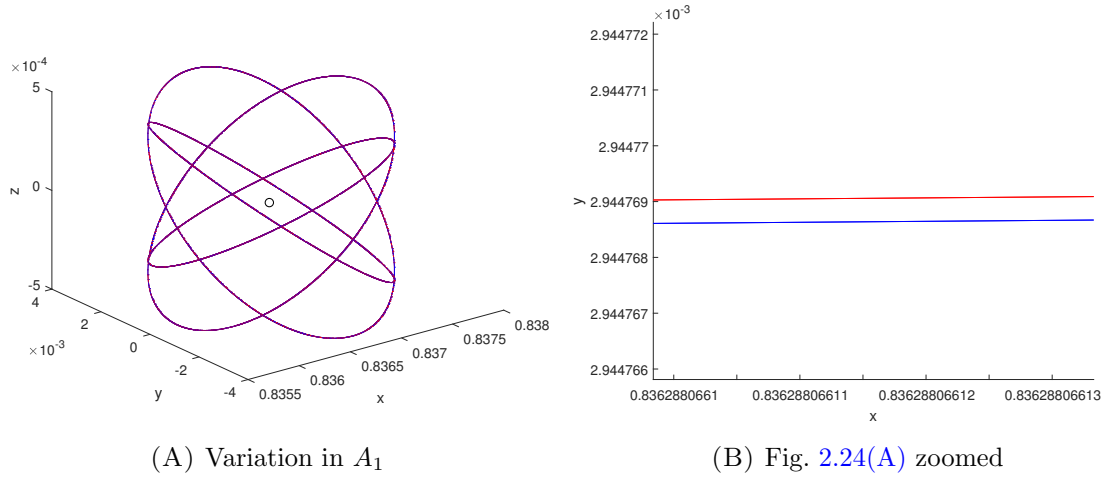


FIGURE 2.24: Effect of oblateness on the size of halo orbits around  $L_1$  in the Earth-Moon system

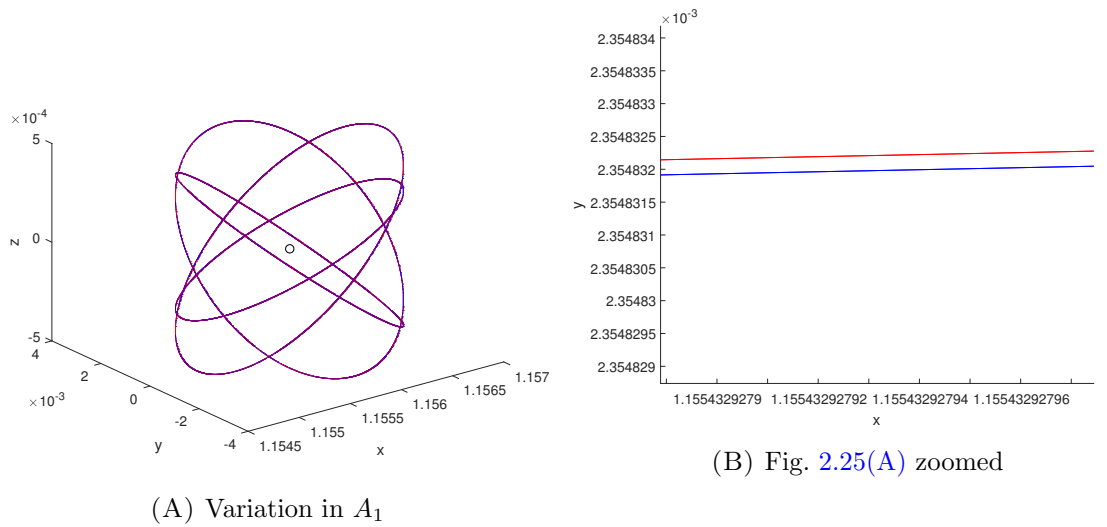


FIGURE 2.25: Effect of oblateness on the size of halo orbits around  $L_2$  in the Earth-Moon system

TABLE 2.7: The third order solution using Differential Correction method around  $L_1$  in the Sun-Earth system

$q_1$	$A_2$	State after One Period					
		$x(\times 10^8)$ (km)	$y$ (km)	$z(\times 10^5)$ (km)	$\dot{x}$ (km/s)	$\dot{y}$ (km/s)	$\dot{z}$ (km/s)
0.99	0	1.482349325923	0.01537829547804	-1.133909213606	-0.000000247024	-0.9379249251592	-0.000000002288
0.979	$2.42405 \times 10^{-12}$	1.480739990796	0.01220841080489	-1.136492221090	-0.00000012061	-0.8697623686843	-0.000000001008
1	$2.42405 \times 10^{-12}$	1.483492814339	-0.01853705437853	-1.139593646274	0.000000043707	-0.97934279615302	0.000000004408
1	0	1.483492814672	-1.696714398844	-1.139593646994	0.000000039550	-0.9834280177174	0.000000003993

TABLE 2.8: The Fourth order solution using Differential Correction method around  $L_1$  in the Sun-Earth system

$q_1$	$A_2$	State after One Period					
		$x(\times 10^8)$ (km)	$y$ (km)	$z(\times 10^5)$ (km)	$\dot{x}$ (km/s)	$\dot{y}$ (km/s)	$\dot{z}$ (km/s)
0.99	0	1.482335599667	0.01515263720041	-1.162260971330	-0.000000243271	-0.9386852200838	-0.000000002311
0.979	$2.42405 \times 10^{-12}$	1.480744116421	0.01283100215901	-1.168284125441	-0.00000012697	-0.8703225978205	-0.000000001095
1	$2.42405 \times 10^{-12}$	1.483496769854	-0.01680695264058	-1.162808055720	0.000000039182	-0.97943331035860	0.000000004039
1	0	1.483496770209	-0.01692211141219	-1.162808055610	0.000000039449	-0.9843331622638	0.000000004066

TABLE 2.9: Fifth order solution using Differential Correction method around  $L_1$  in the Sun-Earth system

$q_1$	$A_2$	State after One Period					
		$x(\times 10^8)$ (km)	$y$ (km)	$z(\times 10^5)$ (km)	$\dot{x}$ (km/s)	$\dot{y}$ (km/s)	$\dot{z}$ (km/s)
0.99	0	1.482353746154	0.01539790921259	-1.163220396318	-0.000000247098	-0.9387112761799	-0.000000002350
0.979	$2.42405 \times 10^{-12}$	1.480744276087	0.01221579325035	-1.169496963821	-0.00000012068	-0.8703442767687	-0.0000000010394
1	$2.42405 \times 10^{-12}$	1.483496895462	-0.01849724911828	-1.163537415879	0.000000043621	-0.97943618389348	0.000000004497
1	0	1.483496895816	-0.01849478525541	-1.163537415825	0.000000043607	-0.9843618974500	0.000000004495

TABLE 2.10: The third order solution using Differential Correction method around  $L_2$  in the Sun-Earth system

$q_1$	$A_2$	State after One Period					
		$x(\times 10^8)$ (km)	$y(\times 10^{-3})$ (km)	$z(\times 10^5)$ (km)	$\dot{x}(\times 10^{-8})$ (km/s)	$\dot{y}$ (km/s)	$\dot{z}(\times 10^{-10})$ (km/s)
0.99	0	1.510824449871	1.471665377223	-1.371615991937	-1.215487480032	-0.9318919070386	9.421767695866
0.979	$2.42405 \times 10^{-12}$	1.509116635243	2.304429951549	-1.355088556281	-3.251103323859	-0.9590569430007	2.946588656184
1	$2.42405 \times 10^{-12}$	1.512856050413	8.898054096977	-1.385564717203	-3.868512472735	-0.900845931123	2.524976983458
1	0	1.512856050318	8.863720985100	-1.385564717258e	-3.854145668884	-0.9008459793949	2.515333632272

TABLE 2.11: The Fourth order solution using Differential Correction method around  $L_2$  in the Sun-Earth system

$q_1$	$A_2$	State after One Period					
		$x(\times 10^8)$ (km)	$y(\times 10^{-3})$ (km)	$z(\times 10^5)$ (km)	$\dot{x}(\times 10^{-8})$ (km/s)	$\dot{y}$ (km/s)	$\dot{z}(\times 10^{-10})$ (km/s)
0.99	0	1.510825131979	1.464787233392	-1.352312958817	-1.212369457842	-0.9313535505452	9.229188944808
0.979	$2.42405 \times 10^{-12}$	1.509117372717	2.248531307499	-1.340918411249	-3.161726609138	-0.9584303866803	2.828363587114
1	$2.42405 \times 10^{-12}$	1.512856519709	8.908057844904	-1.360667549380	-3.873219746086	-0.9003978997643	2.482772448621
1	0	1.512856519610	9.028147554969	-1.360667549302	-3.925456731783	-0.9003979477507	2.516698899572

TABLE 2.12: Fifth order solution using Differential Correction method around  $L_2$  in the Sun-Earth system

$q_1$	$A_2$	State after One Period					
		$x(\times 10^8)$ (km)	$y(\times 10^{-3})$ (km)	$z(\times 10^5)$ (km)	$\dot{x}(\times 10^{-8})$ (km/s)	$\dot{y}$ (km/s)	$\dot{z}(\times 10^{-10})$ (km/s)
0.99	0	1.510825111191	1.501698018895	-1.352905592899	-1.238289982569	-9.313699738583	9.468039282185
0.979	$2.42405 \times 10^{-12}$	1.509117351157	2.261429665733	-1.341334991426	-3.179226343005	-0.9584487219016	2.844869315812
1	$2.42405 \times 10^{-12}$	1.512856504694	8.938490705411	-1.361471740462	-3.885914039301	-9.004122515741	2.492562216162
1	0	1.512856504600	8.905792469188	-1.361471740503	-3.872248085660	-0.9004122998670	2.483556799531

TABLE 2.13: Separation between the third, fourth and fifth order solution around  $L_1$  in the Sun-Earth system

$q_1$	$A_2$	Separation between $3^{rd}$ and $4^{th}$ order analytic solutions (km)	Separation between the $4^{th}$ and $5^{th}$ order analytic solutions (km)	Separation between the $3^{rd}$ and $4^{th}$ order numerical solutions (km)	Separation between the $4^{th}$ and $5^{th}$ order numerical solutions (km)
0.99	0	3693.807761777532	1888.992165744702	2867.206061025634	97.054352043598371
0.979	$2.42405 \times 10^{-12}$	4784.436418469269	1951.606947548718	3205.847725943790	122.3302982814382
1	$2.42405 \times 10^{-12}$	2612.223198770815	1748.091370124659	2354.898955627799	74.0097038858646148
1	0	2612.223184280293	1748.091408386162	2354.899231701449	74.009686186351615

TABLE 2.14: Separation between the third, fourth and fifth order solution around  $L_2$  in the Sun-Earth system

$q_1$	$A_2$	Separation between $3^{rd}$ and $4^{th}$ order analytic solutions (km)	Separation between the $4^{th}$ and $5^{th}$ order analytic solutions (km)	Separation between the $3^{rd}$ and $4^{th}$ order numerical solutions (km)	Separation between the $4^{th}$ and $5^{th}$ order numerical solutions (km)
0.99	0	1907.718409640883	1712.064715234355	1931.508113088076	59.299854276846276
0.979	$2.42405 \times 10^{-12}$	1341.572192391892	1746.621405210147	1418.932269738788	41.713771573529193
1	$2.42405 \times 10^{-12}$	2767.524401687017	1807.106513760034	2490.159040141219	80.433123101888498
1	0	2767.524385678627	1807.106551506953	2490.159045140090	80.433126727805742

TABLE 2.15: Effect of  $q_2$  on different parameters of orbits around  $L_1$  when  $A_1 = A_2 = 0.0002, q_1 = 0.99$

$q_2$	$\gamma$	$L_1$	$C_2$	$C_3$	$C_4$	$C_5$	$C_6$	$\lambda$	$k$	$\Delta$	$\tau$
0.9900	0.107715	0.888284	4.638976	3.082850	3.270704	3.248026	3.250764	2.221946	3.422908	0.298069	2.827784
0.7500	0.098797	0.897202	4.554185	3.058758	3.222699	3.204727	3.206697	2.202616	3.395054	0.297333	2.852600
0.5000	0.087090	0.908909	4.444002	3.023835	3.159317	3.146392	3.147625	2.177230	3.358521	0.296329	2.885861
0.2500	0.070268	0.925731	4.284634	2.964509	3.064283	3.056742	3.057312	2.139955	3.304983	0.294775	2.936128

TABLE 2.16: Effect of  $q_2$  on different parameters of orbits around  $L_2$  when  $A_1 = A_2 = 0.0002, q_1 = 0.99$

$q_2$	$\gamma$	$L_2$	$C_2$	$C_3$	$C_4$	$C_5$	$C_6$	$\lambda$	$k$	$\Delta$	$\tau$
0.9900	0.113481	1.109481	3.487192	-2.845589	2.780199	-2.773535	2.772855	1.942089	3.023335	0.284518	3.235270
0.7500	0.103217	1.099217	3.539441	-2.873621	2.811327	-2.805499	2.804953	1.955708	3.042556	0.285354	3.212741
0.5000	0.089946	1.085946	3.612036	-2.913186	2.855514	-2.850755	2.850362	1.974463	3.069072	0.286470	3.182224
0.2500	0.071272	1.067272	3.727466	-2.978592	2.928769	-2.925454	2.925234	2.003897	3.110787	0.288140	3.135481

TABLE 2.17: Effect of radiation and oblateness on various parameters of orbits in the Sun-Earth system

$A_2$	$q_1$	$\gamma$	$L_3$	$A_z$	$C_2$	$\lambda$	$k$	$\tau$
0	1	0.999998	-1.000001	0.155098703693978	1.000002628066122	1.000002628048856	2.00000000020720	6.283168794705025
	0.99	0.996653	-0.996656	0.155098778099352	1.000002634989055	1.000002634971697	2.00000000020829	6.283168751207761
	0.90	0.965487	-0.965490	0.155099489367699	1.000002701159378	1.000002701141138	2.00000000021888	6.283168335455118
	0.85	0.947266	-0.947269	0.155099920762603	1.000002741285063	1.000002741266277	2.00000000022544	6.283168083342806
0.00005	1	0.999973	-0.999976	0.155091662625958	1.000077628335967	1.000040127517043	2.00000000020721	6.282933188670979
	0.99	0.996628	-0.996631	0.155091737025727	1.000077635259657	1.000040134440383	2.00000000020830	6.282933145173842
	0.95	0.983021	-0.983024	0.155092043533592	1.000077663781697	1.000040162960975	2.00000000021283	6.282932965988065
	0.90	0.965463	-0.965466	0.155092448240049	1.000077701437177	1.000040200614538	2.00000000021889	6.282932729422760
	0.85	0.947242	-0.947245	0.155092879602341	1.000077741567242	1.000040240742552	2.00000000022545	6.282932477311294
0.0001	1	0.999948	-0.999951	0.155084622799540	1.000152628605819	1.000077625579136	2.00000000020722	6.282697609139138
	0.99	0.996603	-0.996606	0.155084697193663	1.000152635530264	1.000077632502971	2.00000000020832	6.282697565642156
	0.95	0.982996	-0.982999	0.155085003678207	1.000152664055406	1.000077661025596	2.00000000021285	6.282697386457044
	0.90	0.965439	-0.965442	0.155085408353976	1.000152701714985	1.000077698681846	2.00000000021891	6.282697149892605
	0.85	0.947219	-0.947222	0.155085839683643	1.000152741849430	1.000077738812735	2.00000000022546	6.282696897781978
0.00015	1	0.999923	-0.999926	0.155077584214286	1.000227628875686	1.000115122235303	2.00000000020723	6.282462056104484
	0.99	0.996579	-0.996582	0.155077658602661	1.000227635800876	1.000115129159623	2.00000000020832	6.282462012607711
	0.95	0.982972	-0.982975	0.155077965063975	1.000227664329122	1.000115157684282	2.00000000021286	6.282461833423261
	0.90	0.965415	-0.965418	0.155078369709038	1.000227701992799	1.000115195343217	2.00000000021892	6.282461596859687
	0.85	0.947195	-0.947198	0.155078801006026	1.000227742131618	1.000115235476975	2.00000000022547	6.282461344749947

TABLE 2.18: Effect of  $A_1$  on different parameters of orbits around  $L_1$  when  $A_2 = 0.0002, q_1 = q_2 = 0.99$

$A_1$	$\gamma$	$L_1$	$C_2$	$C_3$	$C_4$	$C_5$	$C_6$	$\lambda$	$k$	$\Delta$	$\tau$
0.0002	0.107715	0.888284	4.638976	3.082850	3.270704	3.248026	3.250764	2.221946	3.422908	0.298069	2.827784
0.0500	0.103364	0.892635	5.181972	3.514092	3.706365	3.684200	3.686755	2.346038	3.482282	0.321923	2.678210
0.0999	0.099689	0.896310	5.718763	3.940495	4.137399	4.115597	4.118011	2.462604	3.531227	0.345659	2.551438
0.1500	0.096516	0.899483	6.251812	4.364074	4.565736	4.544193	4.546494	2.573166	3.572298	0.369371	2.441810

TABLE 2.19: Effect of  $A_1$  on different parameters of orbits around  $L_2$  when  $A_2 = 0.0002, q_1 = q_2 = 0.99$

$A_1$	$\gamma$	$L_2$	$C_2$	$C_3$	$C_4$	$C_5$	$C_6$	$\lambda$	$k$	$\Delta$	$\tau$
0.0002	0.113481	1.109481	3.487192	-2.845589	2.780199	-2.773535	2.772855	1.942089	3.023335	0.284518	3.235270
0.0500	0.109456	1.105456	3.861428	-3.170963	3.102844	-3.096123	3.095460	2.041807	3.062205	0.307550	3.077265
0.0999	0.105922	1.101922	4.239633	-3.499703	3.428835	-3.422047	3.421397	2.137803	3.096718	0.330571	2.939084
0.1500	0.102779	1.098779	4.622185	-3.832119	3.758485	-3.751622	3.750983	2.230655	3.127649	0.353640	2.816743